



# Uncertainty Analysis of the NASA Glenn 8- by 6-Foot Supersonic Wind Tunnel 2019 Characterization Test 14-Foot, 5.8 Percent Test Section Porosity

*Pamela Poljak*  
*Jacobs Technology, Cleveland, Ohio*

## NASA STI Program . . . in Profile

Since its founding, NASA has been dedicated to the advancement of aeronautics and space science. The NASA Scientific and Technical Information (STI) Program plays a key part in helping NASA maintain this important role.

The NASA STI Program operates under the auspices of the Agency Chief Information Officer. It collects, organizes, provides for archiving, and disseminates NASA's STI. The NASA STI Program provides access to the NASA Technical Report Server—Registered (NTRS Reg) and NASA Technical Report Server—Public (NTRS) thus providing one of the largest collections of aeronautical and space science STI in the world. Results are published in both non-NASA channels and by NASA in the NASA STI Report Series, which includes the following report types:

- **TECHNICAL PUBLICATION.** Reports of completed research or a major significant phase of research that present the results of NASA programs and include extensive data or theoretical analysis. Includes compilations of significant scientific and technical data and information deemed to be of continuing reference value. NASA counter-part of peer-reviewed formal professional papers, but has less stringent limitations on manuscript length and extent of graphic presentations.
- **TECHNICAL MEMORANDUM.** Scientific and technical findings that are preliminary or of specialized interest, e.g., "quick-release" reports, working papers, and bibliographies that contain minimal annotation. Does not contain extensive analysis.
- **CONTRACTOR REPORT.** Scientific and technical findings by NASA-sponsored contractors and grantees.
- **CONFERENCE PUBLICATION.** Collected papers from scientific and technical conferences, symposia, seminars, or other meetings sponsored or co-sponsored by NASA.
- **SPECIAL PUBLICATION.** Scientific, technical, or historical information from NASA programs, projects, and missions, often concerned with subjects having substantial public interest.
- **TECHNICAL TRANSLATION.** English-language translations of foreign scientific and technical material pertinent to NASA's mission.

For more information about the NASA STI program, see the following:

- Access the NASA STI program home page at <http://www.sti.nasa.gov>
- E-mail your question to [help@sti.nasa.gov](mailto:help@sti.nasa.gov)
- Fax your question to the NASA STI Information Desk at 757-864-6500
- Telephone the NASA STI Information Desk at 757-864-9658
- Write to:  
NASA STI Program  
Mail Stop 148  
NASA Langley Research Center  
Hampton, VA 23681-2199



# Uncertainty Analysis of the NASA Glenn 8- by 6-Foot Supersonic Wind Tunnel 2019 Characterization Test 14-Foot, 5.8 Percent Test Section Porosity

*Pamela Poljak*  
*Jacobs Technology, Cleveland, Ohio*

Prepared under Contract NNC15BA02B

National Aeronautics and  
Space Administration

Glenn Research Center  
Cleveland, Ohio 44135

## Acknowledgments

This work was sponsored by the Aerosciences Evaluation and Test Capabilities (AETC) Portfolio at the NASA Glenn Research Center.

Trade names and trademarks are used in this report for identification only. Their usage does not constitute an official endorsement, either expressed or implied, by the National Aeronautics and Space Administration.

*Level of Review:* This material has been technically reviewed by expert reviewer(s).

# Contents

<b>1 Abstract</b>	<b>1</b>
<b>2 Introduction</b>	<b>4</b>
<b>3 Overview</b>	<b>5</b>
3.1 Description of 8- by 6-Foot Supersonic Wind Tunnel . . . . .	5
3.2 2019 Characterization Test . . . . .	6
<b>4 Instrumentation</b>	<b>9</b>
4.1 Facility Instrumentation . . . . .	9
4.2 Calibration Instrumentation . . . . .	9
<b>5 Uncertainty Analysis Overview and Methods</b>	<b>14</b>
5.1 Repeatability Analysis . . . . .	14
5.2 Systematic Uncertainty Analysis . . . . .	15
5.2.1 Systematic Uncertainty Estimates . . . . .	15
5.2.2 Elemental Standard Uncertainty Estimates . . . . .	15
5.2.3 Prediction Model Uncertainty Estimates . . . . .	18
<b>6 Data Reduction</b>	<b>20</b>
<b>7 Results</b>	<b>23</b>
7.1 Mach Number Uncertainty . . . . .	23
7.1.1 Repeatability (Random) Uncertainty Characterization . . . . .	23
7.1.2 Systematic Uncertainty Characterization . . . . .	24
7.1.3 Combined Uncertainty Characterization . . . . .	27
7.2 Systematic Uncertainty Results for Other VOIs . . . . .	28
7.2.1 Static Pressure Systematic Uncertainty . . . . .	28
7.2.2 Total Pressure Systematic Uncertainty . . . . .	31
7.2.3 Dynamic Pressure Systematic Uncertainty . . . . .	34
7.2.4 Total Temperature Systematic Uncertainty . . . . .	36
7.2.5 Static Temperature Systematic Uncertainty . . . . .	38
7.2.6 Test Section Air Speed Systematic Uncertainty . . . . .	40
7.2.7 Reynolds Number Systematic Uncertainty . . . . .	42
<b>8 Conclusions</b>	<b>45</b>
<b>References</b>	<b>49</b>

## List of Figures

1	Overview of 8×6 Supersonic Wind Tunnel and 9×15 Low-Speed Wind Tunnel Complex . . . . .	5
2	Elevation view of 8- by 6-foot test section. . . . .	6
3	Flow chart exhibiting the cascading impacts of characterization tests on variables of interest. . . . .	7
4	Rakes as installed in the bellmouth. . . . .	10
5	Calibration instrumentation: Cone-cylinder . . . . .	10
6	Calibration instrumentation: Transonic array . . . . .	11
7	Schematic of transonic array mounting . . . . .	12
8	Schematic of test section station hardware locations . . . . .	12
9	Factors impacting repeatability at different time scales. . . . .	15
10	Instrumentation level uncertainty analysis flow. . . . .	16
11	Elemental uncertainty estimates for Mensor CPT 6180, 0-15 psia pressure sensor. . . . .	17
12	Elemental uncertainty estimates for Type E thermocouple with special limits of error wire. . . . .	17
13	Mach number data flow chart, subsonic flow range . . . . .	21
14	Mach number data flow chart, supersonic flow range . . . . .	22
15	Random uncertainty in $M_{ts}$ , test section porosity configuration 1 . . . . .	24
16	Systematic uncertainty in $M_{ts}$ , test section porosity configuration 1 . . . . .	25
17	Comparison of systematic uncertainty in $M_{ts}$ , test section porosity configuration 1 . . . . .	26
18	Systematic UPC of $M_{ts}$ , scenario 3, test section porosity configuration 1 . . . . .	26
19	Systematic UPC of $M_{ts}$ , scenario 2, test section porosity configuration 1 . . . . .	27
20	Systematic UPC of $M_{ts}$ , scenario 1, test section porosity configuration 1 . . . . .	27
21	Combined uncertainty in $M_{ts}$ , test section porosity configuration 1 . . . . .	28
22	Systematic uncertainty in $P_{S,ts}$ , test section porosity configuration 1 . . . . .	29
23	Comparison of systematic uncertainty in $P_{S,ts}$ , test section porosity configuration 1 . . . . .	30
24	Systematic UPC of $P_{S,ts}$ , test section porosity configuration 1 . . . . .	30
25	Systematic UPC of $P_{S,ts}$ , scenario 2, test section porosity configuration 1 . . . . .	31
26	Systematic UPC of $P_{S,ts}$ , scenario 1, test section porosity configuration 1 . . . . .	31
27	Systematic uncertainty in $P_{T,ts}$ , test section porosity configuration 1 . . . . .	32
28	Comparison of systematic uncertainty in $P_{T,ts}$ , test section porosity configuration 1 . . . . .	32
29	Systematic UPC of $P_{T,ts}$ , scenario 3, test section porosity configuration 1 . . . . .	33
30	Systematic UPC of $P_{T,ts}$ , scenario 2, test section porosity configuration 1 . . . . .	33
31	Systematic UPC of $P_{T,ts}$ , scenario 1, test section porosity configuration 1 . . . . .	33
32	Systematic uncertainty in $Q_{ts}$ , test section porosity configuration 1 . . . . .	34
33	Systematic UPC of $Q_{ts}$ , scenario 3, test section porosity configuration 1 . . . . .	35
34	Systematic UPC of $Q_{ts}$ , scenario 2, test section porosity configuration 1 . . . . .	35
35	Systematic UPC of $Q_{ts}$ , scenario 1, test section porosity configuration 1 . . . . .	35
36	Systematic uncertainty in $T_{T,ts}$ , test section porosity configuration 1 . . . . .	36
37	Comparison of systematic uncertainty in $T_{T,ts}$ , test section porosity configuration 1 . . . . .	37
38	Systematic UPC of $T_{T,ts}$ , scenario 3, test section porosity configuration 1 . . . . .	37
39	Systematic UPC of $T_{T,ts}$ , scenario 2, test section porosity configuration 1 . . . . .	38
40	Systematic UPC of $T_{T,ts}$ , scenario 1, test section porosity configuration 1 . . . . .	38
41	Systematic uncertainty in $T_{S,ts}$ , test section porosity configuration 1 . . . . .	39
42	Systematic UPC of $T_{S,ts}$ , scenario 3, test section porosity configuration 1 . . . . .	39
43	Systematic UPC of $T_{S,ts}$ , scenario 2, test section porosity configuration 1 . . . . .	40
44	Systematic UPC of $T_{S,ts}$ , scenario 1, test section porosity configuration 1 . . . . .	40
45	Systematic uncertainty in $U_{ts}$ , test section porosity configuration 1 . . . . .	41
46	Systematic UPC of $U_{ts}$ , scenario 3, test section porosity configuration 1 . . . . .	41
47	Systematic UPC of $U_{ts}$ , scenario 2, test section porosity configuration 1 . . . . .	42
48	Systematic UPC of $U_{ts}$ , scenario 1, test section porosity configuration 1 . . . . .	42
49	Systematic uncertainty in $RE_{ft}$ , test section porosity configuration 1 . . . . .	43
50	Systematic UPC of $RE_{ts}$ , scenario 3, test section porosity configuration 1 . . . . .	43
51	Systematic UPC of $RE_{ft}$ , scenario 2, test section porosity configuration 1 . . . . .	44
52	Systematic UPC of $RE_{ft}$ , scenario 1, test section porosity configuration 1 . . . . .	44

## List of Tables

I	Test section configuration descriptions . . . . .	6
II	Facility condition settings for prediction model scenarios . . . . .	7
III	Critical facility instrumentation measurements . . . . .	13
IV	Critical calibration instrumentation measurements . . . . .	13
V	Uncertainty estimates for critical measurements and measurement systems . . . . .	17
VI	Static pressure prediction model uncertainty estimates . . . . .	18
VII	Total pressure prediction model uncertainty estimates . . . . .	18
VIII	Total temperature prediction model uncertainty estimates . . . . .	19
IX	Mach Number, Summary of Random Uncertainty Results, test section porosity configuration 1	24
X	Mach Number, Summary of Systematic Uncertainty Results, scenario 3, test section porosity configuration 1 . . . . .	27
XI	Mach Number, Summary of Combined Uncertainty Results, scenario 3, test section porosity configuration 1 . . . . .	28
XII	Static Pressure, Summary of Systematic Uncertainty Results, scenario 3, test section porosity configuration 1 . . . . .	31
XIII	Total Pressure, Summary of Systematic Uncertainty Results, test section porosity configuration 1 . . . . .	33
XIV	Dynamic Pressure, Summary of Systematic Uncertainty Results, test section porosity configuration 1 . . . . .	35
XV	Total Temperature, Summary of Systematic Uncertainty Results, Scemario 3, test section porosity configuration 1 . . . . .	38
XVI	Static Temperature, Summary of Systematic Uncertainty Results, test section porosity configuration 1 . . . . .	40
XVII	Air speed, Summary of Systematic Uncertainty Results, scenario 3, test section porosity configuration 1 . . . . .	42
XVII	Reynolds Number, Summary of Systematic Uncertainty Results, scenario 3, test section porosity configuration 1 . . . . .	44
XIX	Summary of Systematic Uncertainty Results, configuration 1 . . . . .	45
XX	Uncertainty ( $k=2$ ) Look-Up Table, Supersonic Localized Prediction Model With $P_S$ correction . . . . .	46
XXI	Uncertainty ( $k=2$ ) Look-Up Table, Supersonic Localized Prediction Model . . . . .	47
XXII	Uncertainty ( $k=2$ ) Look-Up Table, Generalized Prediction Model . . . . .	48



# **Uncertainty Analysis of the NASA Glenn 8- by 6-Foot Supersonic Wind Tunnel 2019 Characterization Test 14-Foot, 5.8 Percent Test Section Porosity**

Pamela Poljak  
Jacobs Technology  
Cleveland, Ohio 44135

## **1 Abstract**

This Contractor Report presents methods and results of a measurement uncertainty analysis that was performed for the 8- by 6-Foot Supersonic Wind Tunnel located at the NASA Glenn Research Center. The uncertainty analysis is based on data collected during a characterization test following major structural modifications to the facility and upgrades to the facility's data and control systems. The statistical methods and engineering judgments used to estimate elemental uncertainties are described in this report. The Monte Carlo method of propagating uncertainty was selected to determine the uncertainty of calculated variables of interest. A description of the Monte Carlo method as applied for this analysis is provided.

The primary variable of interest (VOI) for this facility is free stream Mach number. In addition to determining the uncertainty in Mach number, the uncertainty in free stream values of static pressure, total pressure, dynamic pressure, total temperature, static temperature, Reynolds number, and air speed were also calculated. Uncertainty results are presented as random (unpredictable variation in repeated measurements), systematic (potential offset between observed and true value), and total (random and systematic combined) uncertainty for Mach number. Systematic uncertainty results are presented for the other VOIs. Individual uncertainty sources are presented both dimensionally and as percent contributions to uncertainty in all VOIs, to aid in the identification of primary uncertainty sources.

## Nomenclature

$\gamma$	Ratio of specific heats
$\mu$	Air viscosity, <i>slugs/(ft · sec)</i>
$\rho$	Air density, <i>slugs/ft<sup>3</sup></i>
$^{\circ}R$	Rankine
$A_{0-3}$	Static pressure calibration generalized prediction model coefficients, subsonic flow
$A_{S0-S4}$	Static pressure calibration localized prediction model coefficients, supersonic flow
$A_{SX0-SX4}$	Static pressure calibration on-nominal prediction model coefficients, supersonic flow
$B_x$	Expanded systematic uncertainty of variable $x$
$b_x$	Standard systematic uncertainty of variable $x$
$B_{0-3}$	Total pressure calibration generalized prediction model coefficients, subsonic flow
$B_{S0-S3}$	Total pressure calibration localized prediction model coefficients, supersonic flow
$B_{SX0-SX2}$	Total pressure calibration on-nominal prediction model coefficients, supersonic flow
$ESPREF$	Barometric reference pressure, <i>psia</i>
$k$	Coverage factor
$M_{ts,subsonic}$	Subsonic Mach number during testing
$M_{ts,supersonic}$	Supersonic Mach number during testing
$P5[2 - 4][7 - 10]$	Transonic array total pressure, 7 innermost, centerline, <i>psia</i>
$P_S$	Static pressure, <i>psia</i>
$P_T$	Total pressure, <i>psia</i>
$P_{bar}$	Barometric reference pressure, <i>psia</i>
$P_{S,bal,1-4}$	Balance chamber static pressure measurements, <i>psia</i>
$P_{S,bal,cal}$	Average balance chamber static pressure measured during calibration, <i>psia</i>
$P_{S,bal,test}$	Balance chamber static pressure during testing, <i>psia</i>
$P_{S,cyl,60}$	Four-inch cone cylinder, 60 aft static pressure measurements, <i>psia</i>
$P_{S,cyl,cal}$	Average cone cylinder static pressure measured during calibration, <i>psia</i>
$P_{S,ts}$	Test section static pressure, <i>psia</i>
$P_{T,2,ts}$	Test section total pressure behind normal shock during testing, <i>psia</i>
$P_{T,2}$	Total pressure measured downstream of a normal shock, <i>psia</i>
$P_{T,arr,2-4,7-10}$	Transonic array total pressure measurements, <i>psia</i>
$P_{T,arr,cal}$	Average transonic array total pressure measured during calibration, <i>psia</i>
$P_{T,bm,1-8}$	Bellmouth rake total pressure measurements, <i>psia</i>
$P_{T,bm,cal}$	Average bellmouth total pressure measured during calibration, <i>psia</i>

$P_{T,bm,test}$	Bellmouth total pressure during testing, psia
$P_{T,ts}$	Test section total pressure, psia
$PSBAL[1 - 4]$	Balance chamber static pressure, <i>psia</i>
$PSCCR1[29 - 51]$	4-inch cone cylinder static pressure, row 1, <i>psia</i>
$PSCCR2[29 - 51]$	4-inch cone cylinder static pressure, row 2, <i>psia</i>
$PSCCR3[7 - 15]$	4-inch cone cylinder static pressure, row 3, <i>psia</i>
$PSCCR4[7 - 15]$	4-inch cone cylinder static pressure, row 4, <i>psia</i>
$PTBM[1 - 8]$	Bellmouth total pressure, <i>psia</i>
$q$	Dynamic pressure, <i>psia</i>
$R_{S,arr,bm,cal}$	Ratio between transonic array total pressure and bellmouth total pressure during calibration
$R_{S,bal,bm,cal}$	Ratio between balance chamber static pressure and bellmouth total pressure during calibration
$R_{S,bal,bm}$	Ratio between balance chamber static pressure and bellmouth total pressure
$R_{S,cyl,bm,cal}$	Ratio between 4-inch cone cylinder static pressure and bellmouth total pressure during calibration
$Re$	Reynolds number, $ft^{-1}$
$S_x$	Expanded random uncertainty of variable $x$
$T_S$	Static temperature, <i>Rankine</i>
$T_T$	Total temperature, <i>Rankine</i>
$TCREF$	Reference temperature, <i>Rankine</i>
$TTBM[1 - 4]$	Bellmouth total temperature, <i>Rankine</i>
$TTTA[3 - 9]$	Transonic array total temperature, 7 innermost, centerline, <i>Rankine</i>
$U$	Free stream air speed, $ft/s$
$U_x$	Expanded combined uncertainty of variable $x$
M	Mach number
MCM	Monte Carlo Method
TSM	Taylor Series Method
VOI	Variable of interest
<i>arr</i>	Designates transonic array (calibration hardware) as location of measurement
<i>bal</i>	Designates balance chamber as location of measurement
<i>bar</i>	Designates barometric (pressure)
<i>bm</i>	Designates bellmouth (entry to contraction) as location of measurement
<i>cyl</i>	Designates cone-cylinder (calibration hardware) as location of measurement
<i>ts</i>	Designates 8- by 6-foot test section as location of calculated variable of interest

## 2 Introduction

This Contractor Report details the measurement uncertainty analysis performed for the NASA Glenn 8- by 6-Foot Supersonic Wind Tunnel ( $8 \times 6$  SWT) following major structural upgrades, between 2016 and 2019, to the  $8 \times 6$  SWT and 9- by 15-Foot Low-Speed Wind Tunnel ( $9 \times 15$  LSWT) complex and to the facility data and control systems. Data used for this analysis were obtained during a series of characterization test runs in the  $8 \times 6$  SWT in 2019. A detailed description of the modifications to the facility can be found in Section 1 of the characterization test report, *Characterization of the NASA Glenn Research Center 8- by 6-Foot Supersonic Wind Tunnel (2019 Test)* (Ref. [1]).

The uncertainty analysis was performed in 2022. The objective was to determine the uncertainty in the primary VOI, free stream Mach number, as well as uncertainties in other free stream VOIs (static pressure, total pressure, dynamic pressure, static temperature, total temperature, Reynolds number, and airspeed). In addition to determining the overall uncertainties, the elemental contributors that drive these uncertainties were also identified.

The document provides background information on the facility, including a brief description of the facility and how it operates, as well as the calibration procedure used to define the free stream conditions. The uncertainty sources considered in this analysis are defined, and a description of the ways in which these uncertainties were propagated is given. A summary of the results is presented and discussed.

### 3 Overview

#### 3.1 Description of 8- by 6-Foot Supersonic Wind Tunnel

The 8×6 SWT and 9×15 LSWT complex, shown in Figure 1, is an atmospheric pressure, continuous flow propulsion wind tunnel. Airflow through the facility is driven by a seven-stage compressor powered by three 29,000-hp electric motors. The 8- by 6-foot test section is a porous-wall, transonic test section with a Mach number range of 0.25 to 2.0. The 9×15 LSWT test section is located in the return leg of the 8×6 SWT loop.

The 8×6 SWT test section walls, flow and ceiling have no divergence over the test section length. The test section is divided into two testing sections: a solid wall supersonic flow region 9 feet 1 inch in length, and a porous wall transonic region 14 feet 5 inches in length. An elevation view of the 23-foot-long test section is shown in Figure 2.

There are six configurations for the transonic test section based on the length of the porous area used and the open area of the test section surfaces. A seventh configuration exists for testing within the solid-wall supersonic test section with the transonic test section configured as defined in Table I.

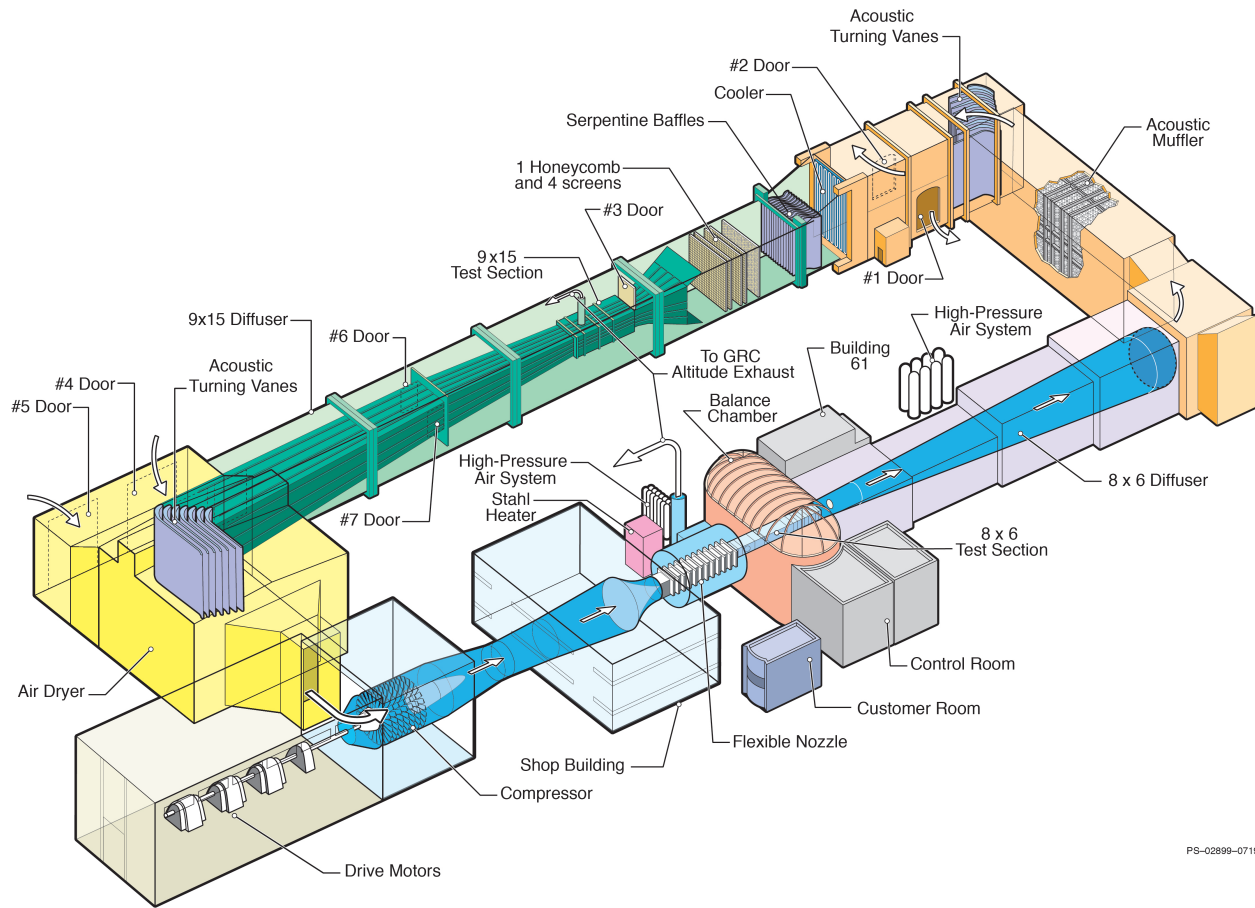


Figure 1. Overview of 8×6 SWT and 9×15 LSWT complex following 9×15 LSWT acoustic improvement modifications.

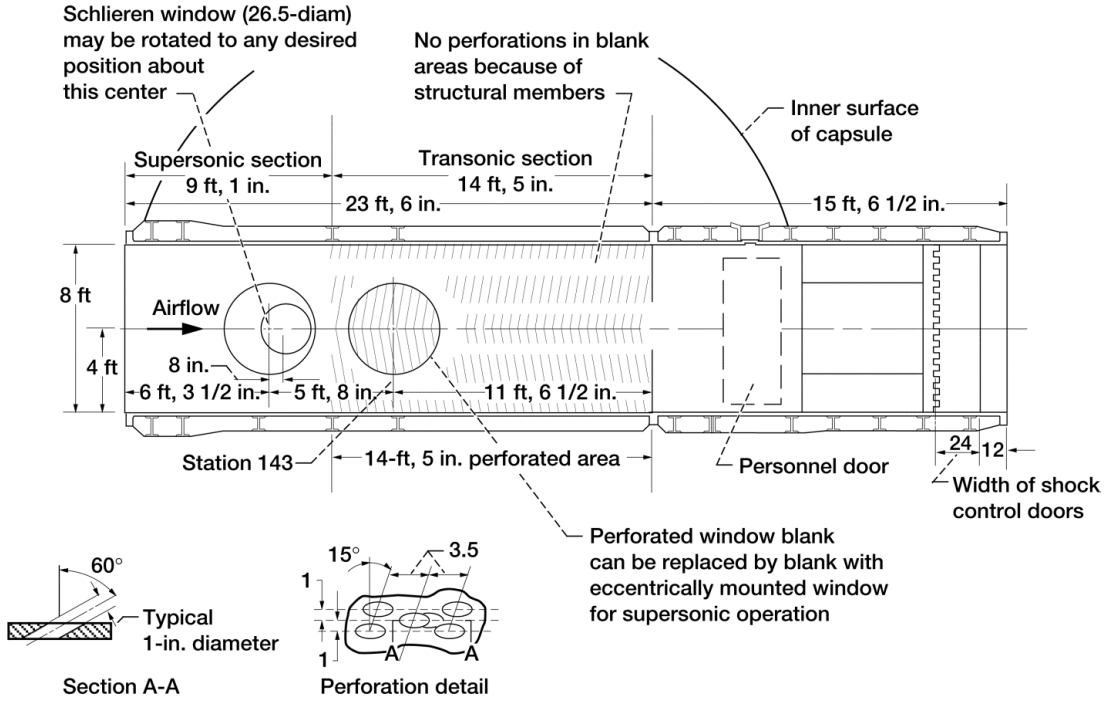


Figure 2. Elevation view of 8- by 6-foot test section.

TABLE I. TEST SECTION CONFIGURATION DESCRIPTIONS

Configuration	Description
1	14-ft, 5.8-percent-porosity
2	8-ft, 6.2-percent-porosity
3	8-ft, 3.1-percent-porosity
4	8-ft, 6.2-percent-porosity modified
5	8-ft, 3.1-percent-porosity modified
6	14-ft, Schlieren windows installed
7	Supersonic test section (transonic test section configured to 8-ft, 6.2-percent porosity)

### 3.2 2019 Characterization Test

Major structural modifications were made to the 8×6 SWT and 9×15 LSWT complex between 2016 and 2019, along with upgrades to the facility's data and control systems. In 2019, a characterization test (Ref. [1]) was run in the 8×6 SWT following the modifications.

The characterization test included calibrations to relate free stream behavior (nearly empty test section) to facility measurements that can be taken with or without a model present in the test section. Data is taken in both the facility and test section during a calibration, and a curve fit relating the two is created. Facility-to-test-section relationships for static pressure ( $P_{S,ts}$ ), total pressure ( $P_{T,ts}$ ), total pressure downstream of a normal shock ( $P_{T,2,ts}$ ), and total temperature ( $T_{T,ts}$ ) were generated from the characterization test data. During a test, when customers are obtaining data from their model, test section conditions are determined by the facility data and calibration coefficients.

When operating the tunnel, nominal conditions for compressor speed, flexible wall position, and shock door positions are set. The ratio of the balance chamber static to bellmouth total pressures is also set to a nominal value based on the tables in the facility operations manual (Ref. [2]). This pressure ratio, defined as

$$R_{S,bal,bm} = \frac{P_{S,bal}}{P_{T,bm}}, \quad (1)$$

is achieved and maintained via active control of a bleed valve in the balance chamber. In addition to the nominal conditions scenario, data were taken for two combinations of off-nominal conditions over the supersonic operating range. The scenarios are shown Table II.

In scenarios 1 and 2, at each nominal flexwall position, a unique prediction model was developed, which is valid over a specified  $R_{S,bal,bm}$  range. In scenario 1, when  $R_{S,bal,bm}$  is within  $\pm 0.0005$  of the nominal condition, an additional correction factor is added to the static pressure prediction. The prediction model for scenario 3 is a generalized curve that covers the entire Mach range, as a whole. The generalized prediction model typically applies when operators are changing condition and the flexwall position and pressure ratio are shifting. Uncertainty predictions were developed for each case separately.

The static pressure calibration relates facility parameters  $P_{T,bm}$  and  $R_{S,bal,bm}$  to test section static pressure. The total pressure calibration relates facility parameters  $P_{T,bm}$  and  $R_{S,bal,bm}$  to test section total pressure for subsonic and supersonic flow ranges, respectively. The average of the innermost seven total pressure readings taken at the centerline vertical array height by the transonic array (see Figure 6), defined as  $P_{T,arr}$ , was used to represent test section total pressure  $P_{T,ts}$  during calibration. Note that in supersonic flow, the measurement observed by a probe is the total pressure downstream of the normal shock produced by the probe, denoted by  $P_{T,2}$ .

Likewise, the total temperature calibration relates facility temperature  $T_{T,bm}$  and  $R_{S,bal,bm}$  to test section temperature. An average of the seven innermost total temperature readings taken at the centerline vertical array height, defined as  $T_{T,arr}$ , was used to represent test section total temperature  $T_{T,ts}$ .

The cascading influence of these tests on one another is shown in Figure 3.

**TABLE II. FACILITY CONDITION SETTINGS FOR PREDICTION MODEL SCENARIOS**

Scenario	Flexwall Position	$R_{S,bal,bm}$	Descriptor
1	within $\pm 2$ deg of nominal setpoint	within $\pm 0.0005$ of nominal setpoint	On-nominal
2	within $\pm 2$ deg of nominal setpoint	within nominal setpoint boundaries	Localized
3	outside nominal setpoint boundaries	outside nominal setpoint boundaries	Generalized

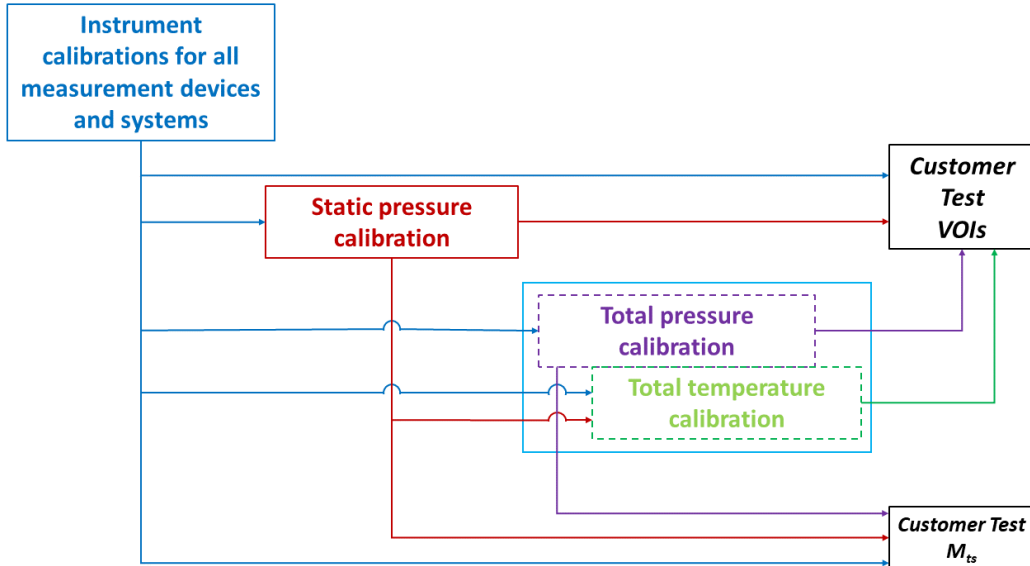


**Figure 3. Flow chart exhibiting the cascading impacts of characterization tests on variables of interest.**

Detailed descriptions of the characterization test setup, operational procedures and test matrices used during the 2019 test entry are contained in Section 4 of the 2019 characterization test report (Ref. [1]). Refer to Sections 5 and 6 of the report for information regarding data reduction methodologies and development of calibration models.

## 4 Instrumentation

### 4.1 Facility Instrumentation

The facility operating conditions are set by controlling compressor speed, flexible wall position, balance chamber pressure (test section bleed), and shock door position. The setpoint is determined predominantly by the ratio of the static pressure in the balance chamber to the total pressure in the bellmouth (the contraction directly upstream of the flexwall). To obtain these measurements, four static pressure measurements are taken at various locations in the balance chamber and are averaged to give  $P_{S,bal}$ . Two wall-mounted rakes near the exit of the bellmouth on the north and south tunnel walls acquire four total pressures and two total temperatures each. The eight total pressure measurements are averaged to give  $P_{T,bm}$  and three of the total temperature measurements are averaged to give  $T_{T,bm}$ . All pressures measured are differential and are added to measured barometric pressure  $P_{bar}$  to give absolute pressures. Unless otherwise noted, pressures are quoted in psia and temperatures in degrees Rankine. More details on the facility operation can be found in the facility manual (Ref. [2]). A schematic of the bellmouth is shown in Figure 4. A list of critical facility instrumentation is shown in Table III.

### 4.2 Calibration Instrumentation

The calibration instrumentation used to collect test section data consisted of a cone-cylinder and a transonic array. The 4-inch diameter, 86-inch long cone-cylinder shown in Figure 5 has four rows of static pressure taps: rows 1 and 2 have 51 static taps each, rows 3 and 4 have 15 static taps each.

The instrumentation on the transonic array includes five 5-hole flow angularity probes, six Pitot-static probes and 11 thermocouples. A schematic of the instrumentation on the array is shown in Figure 6. The array is sting-mounted to a transonic strut in the facility and has wall plates at both ends for additional support, as shown in Figure 7. The vertical height of the array can be set to five different heights, from 24 to 72 inches in 12-inch increments as shown, with 48 inches being the tunnel centerline. The axial position of the array is also variable, as shown in Figure 8. For configurations 1 and 6, the 138.4-inch station is used, placing the centerline of the flow angularity probes approximately at the centerline of the Schlieren window blanks. All other configurations place the array at the 171.4-inch axial station so that the probe measurement plane is at the inlet of the 8-foot test section. There is a third axial position used for tunnel characterization at the 246-inch station, which is not used for calibration. A list of critical calibration instrumentation is shown in Table IV.

Detailed descriptions of the 2019 characterization test instrumentation and test hardware can be found in Section 3 of the 2019 characterization test report (Ref. [1]).

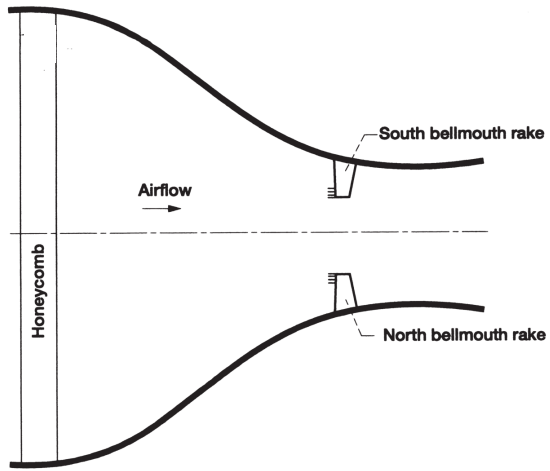


Figure 4. Rakes as installed in the bellmouth.

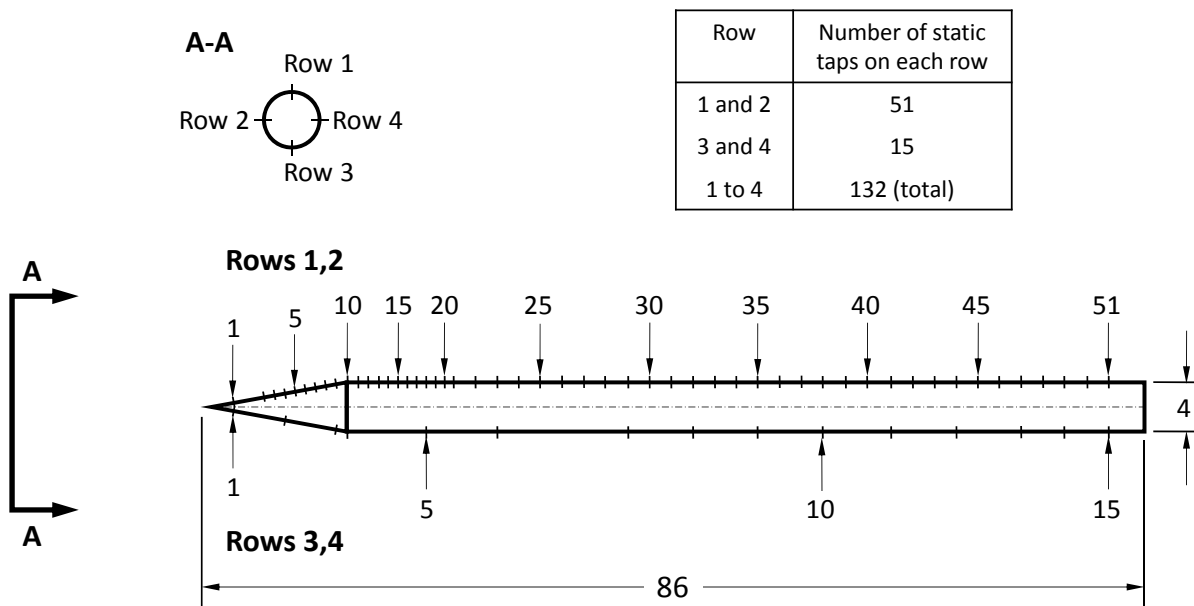


Figure 5. Instrumentation for the 4-inch cone-cylinder used during calibration. All dimensions in inches.

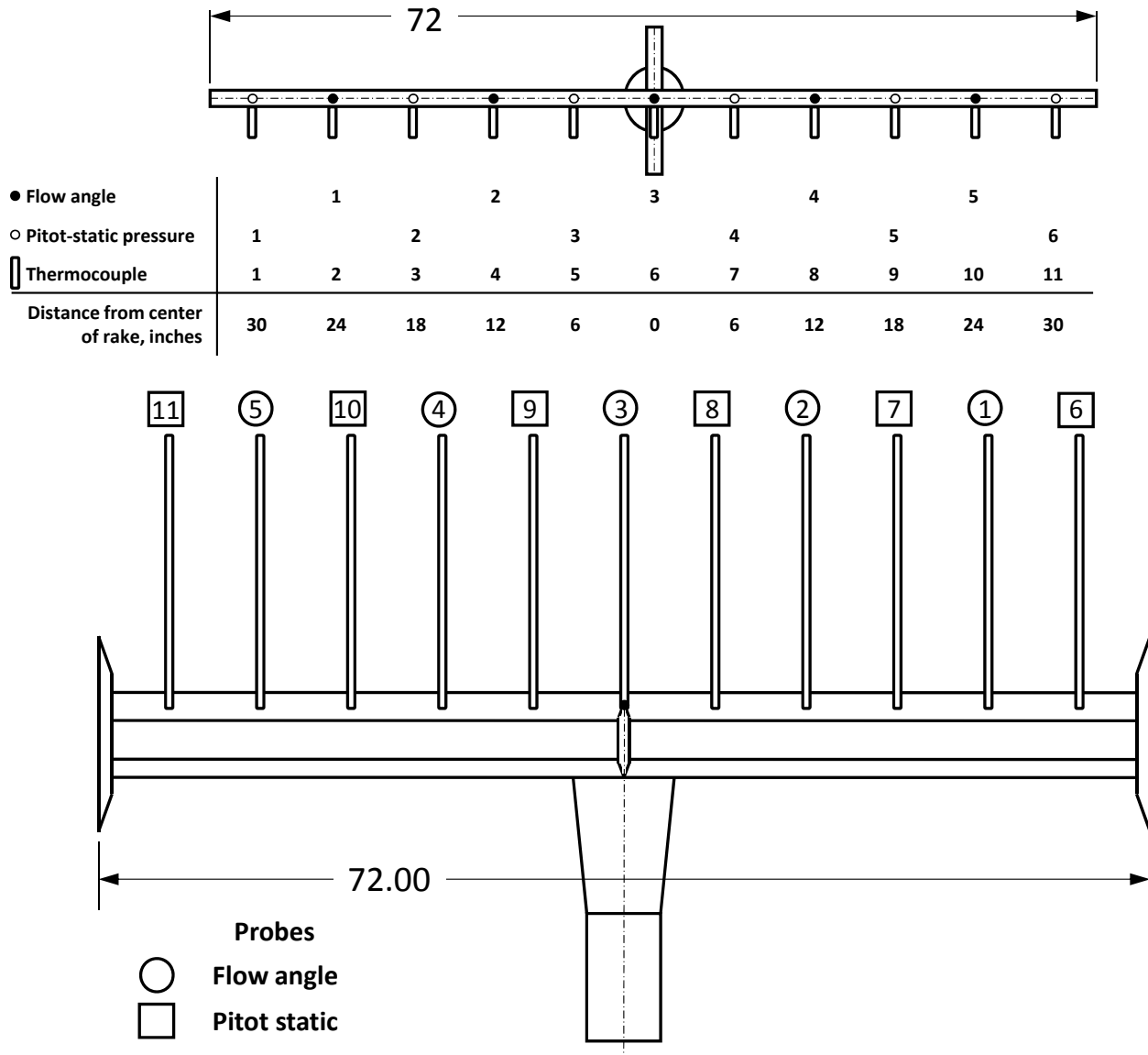


Figure 6. Instrumentation on the transonic array used during calibration. All dimensions are in inches.

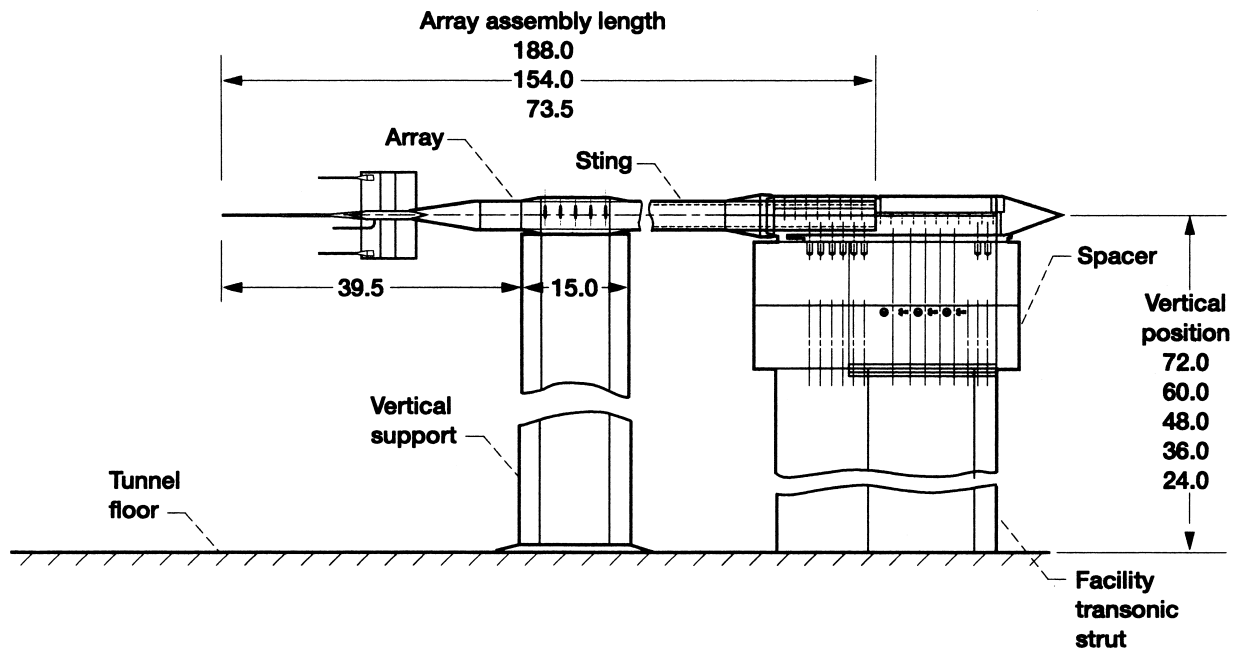


Figure 7. Schematic of transonic array as sting-mounted in the test section for calibration. All dimensions are in inches.

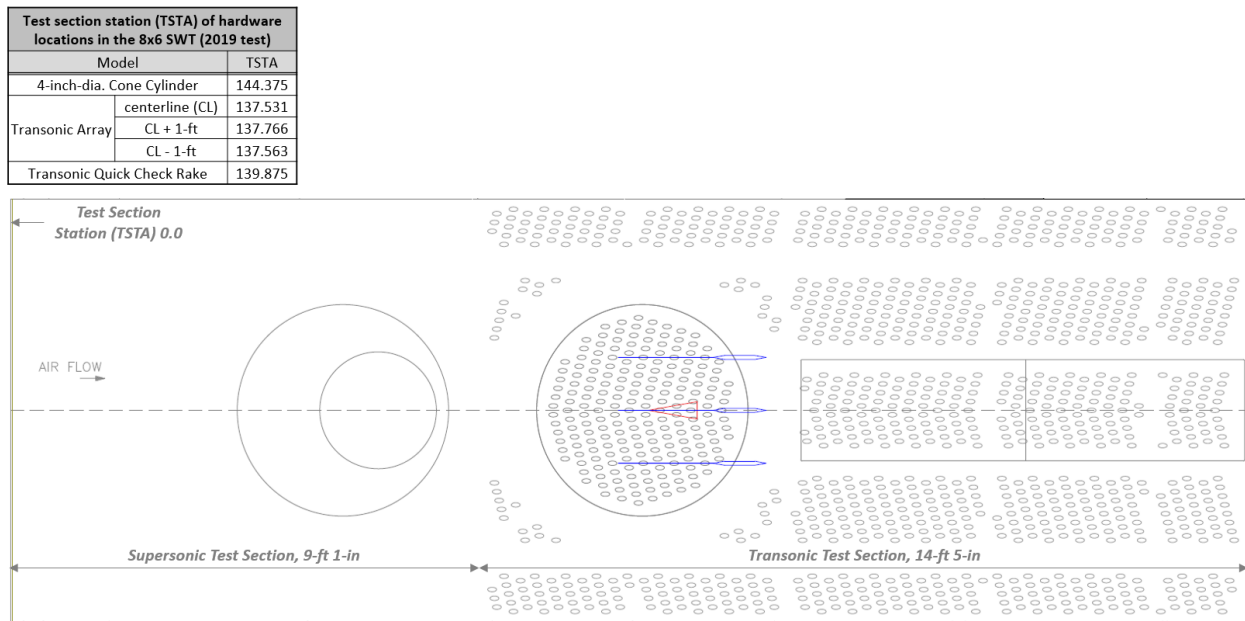


Figure 8. Test section station of hardware locations in the 8×6 SWT (2019 test). Dimensions are in inches and feet.

**TABLE III. CRITICAL FACILITY INSTRUMENTATION MEASUREMENTS**

<b>Variable Name</b>	<b>Description</b>	<b>Units</b>	<b>Measurement System</b>
<i>ESPREF</i>	Barometric reference pressure	psia	Mensor CPT 6180, 0-15 psia <sup>1</sup>
<i>TCREF</i>	Reference temperature	Rankine	Kaye UTR/Fluke Blackstack
<i>PTBM[1 – 8]</i>	Bellmouth total pressure	psia	Optimus DTC, ±15 psid module, barometric reference
<i>PSBAL[1 – 4]</i>	Balance chamber static pressure	psia	Optimus DTC, ±15 psid module, barometric reference
<i>TTBM[1 – 4]</i>	Plenum total temperature	Rankine	Type E thermocouple, Kaye UTR/Fluke BlackStack

**TABLE IV. CRITICAL CALIBRATION INSTRUMENTATION MEASUREMENTS**

<b>Variable Name</b>	<b>Description</b>	<b>Units</b>	<b>Measurement System</b>
<i>PSCCR1[29 – 51]</i>	4-inch cone cylinder static pressure, row 1 <sup>2</sup>	psia	Optimus DTC, ±15 psid module, barometric reference
<i>PSCCR2[29 – 51]</i>	4-inch cone cylinder static pressure, row 2 <sup>2</sup>	psia	Optimus DTC, ±15 psid module, barometric reference
<i>PSCCR3[7 – 15]</i>	4-inch cone cylinder static pressure, row 3 <sup>2</sup>	psia	Optimus DTC, ±15 psid module, barometric reference
<i>PSCCR4[7 – 15]</i>	4-inch cone cylinder static pressure, row 4 <sup>2</sup>	psia	Optimus DTC, ±15 psid module, barometric reference
<i>P5[[2 – 4][7 – 10]]</i>	Transonic array total pressure, 7 innermost, centerline	psia	Optimus DTC, ±15 psid module, barometric reference
<i>TTTA[3 – 9]</i>	Transonic array total temperature, 7 innermost, centerline	Rankine	Type E thermocouple, Kaye UTR/Fluke BlackStack

<sup>1</sup>The Optimus DTC pressure measurement system measures differential pressure. Barometric reference pressure, *ESPREF*, is added to each Optimus pressure measurement to result in absolute pressure.

<sup>2</sup>Pressure port stations 40 inches or more downstream of cone tip.

## 5 Uncertainty Analysis Overview and Methods

Following the classification scheme in the ASME and AIAA uncertainty standards and guides (Refs. [3] and [4]), uncertainty estimates are broken down into two main categories: random and systematic. This classification scheme helps to identify how the types of uncertainty can be best estimated and how they can be expected to affect data and subsequent calculations. Random uncertainty characterizes variation that is inherent to taking data in the real world. Environmental fluctuations, electrical noise, vibrations, variation in uncontrolled parameters, etc. are common sources of random uncertainty. Systematic uncertainty characterizes the biases that occur in measurements due to instrument behavior (non-linearity, hysteresis, etc.), instrument and model installation effects, data reduction choices, manufacturing quality, human operation, test procedures, etc.

Both uncertainty types affect data, present challenges, and require distinct estimation techniques. Random uncertainty sources are difficult or impossible to isolate from one another; however, their combined effects are observable and readily estimable if repeated measurements are obtained at the same nominal conditions and statistical analyses are performed. Random uncertainty, synonymous with repeatability, causes scatter in data about some mean value and generally can be assumed to follow a Gaussian distribution. If a researcher is interested in the average value of a parameter, the level of random uncertainty can be diminished by obtaining and averaging multiple readings or samples.

Systematic uncertainty sources may be easy to identify conceptually, but are often difficult, time-consuming, and/or expensive to quantify. Because they result in a bias, repeated measurements at the same nominal conditions would all contain similar bias with no clues as to the level of offset from the true value of the measurement. If it is possible to quantify a bias effect through a controlled test, a correction is made to eliminate its impact on the data. A common example of this is a pressure measurement being corrected for a change in temperature of the transducer, called a temperature compensation. If it is not possible to quantify a bias effect, estimates of significant systematic uncertainty sources must be made and analytically propagated to VOIs. Most often, this is performed via the Monte Carlo Method (MCM) or Taylor Series Method (TSM) of uncertainty propagation. Systematic uncertainty sources can follow different probability distributions and are often unknown. If a researcher is interested in a comparison of a computational fluid dynamics (CFD) solution to experimental results, systematic uncertainty in both must be well understood before conclusions can be drawn about the agreement between the two results.

Correlated uncertainty arises when an error source impacts two or more measurements. Measurements that share a common excitation voltage source or a common reference junction are two examples of correlated uncertainty.

### 5.1 Repeatability Analysis

Repeatability conceptually represents how consistently a measurement can be replicated. More technically, repeatability quantifies the level of variation observed in a parameter when a test point is repeated several times. The term is used interchangeably with random uncertainty throughout this document. This random variation can be assumed to follow a Gaussian or near-Gaussian distribution by the Central Limit Theorem (Ref. [5]), as it results from many different (and often indistinguishable) sources. It is therefore useful to define repeatability in relation to a common statistical parameter: the standard deviation of a population,  $\sigma$ . This is a widely understood metric, as the “2-sigma” value represents a 95 percent coverage interval about the population average in a Gaussian distributed population. Factors that contribute to random uncertainty differ depending on the time scale over which the repeated measurements are obtained, making time scale a critical component to both quantifying and reporting repeatability. There are three distinct time scales that are useful to analyze: short-term (“back-to-back” or cyclic data), near-term (“within-test” or data taken over hours, days, or weeks), and long-term (“between-test” or data taken over months or years). Each of these time scales captures a different scope of variability. Short-term repeatability captures variation at the instrument level, near-term repeatability captures variation at the facility level, while long-term repeatability captures variation at the process level. Figure 9 lists some of the factors given that impact variability for these time scales. In general, the level of variation increases as the time scale increases since more sources of variation tend to become influential as time passes.

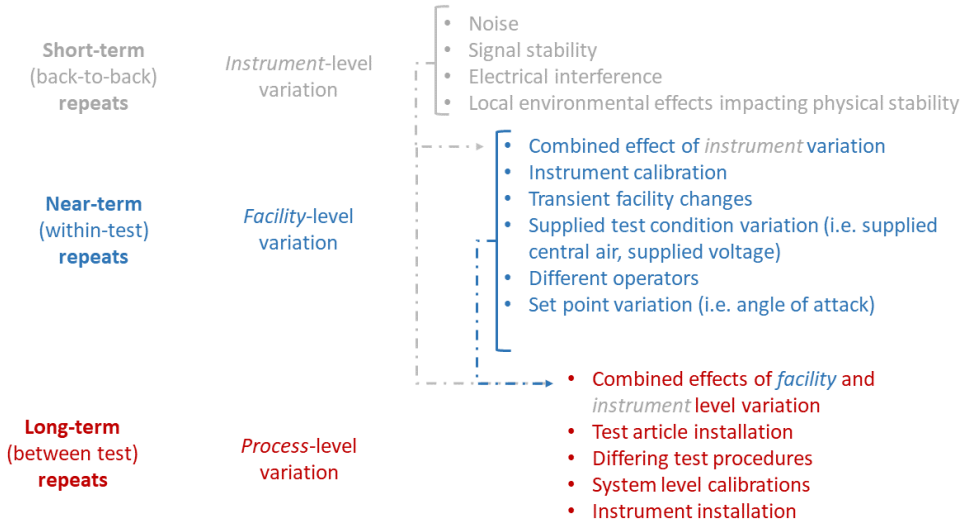


**Figure 9. Factors impacting repeatability at different time scales.**

Random uncertainty was quantified for the 2019 Characterization Test as “within-test,” i.e., in a near-term time scale for this test. Repeat conditions were acquired with the 4-inch-diameter cone cylinder and transonic array at test section centerline at each nominal supersonic Mach number setting in 0.1 Mach increments (Ref. [1]).

## 5.2 Systematic Uncertainty Analysis

### 5.2.1 Systematic Uncertainty Estimates

The Monte Carlo Method (MCM) of uncertainty propagation was selected to further propagate systematic measurement uncertainties through a simulation of the data reduction sequences listed in Section 6 . In brief, the MCM allows one to simulate tens of thousands of “synthetic realizations” of a test point, test matrix, or sequence of tests. As best as possible, the Monte Carlo simulation implements error population properly based on assumed error distributions, uncertainty correlations between measurements, and uncertainty correlations between test entries. Using uncertainty estimates, appropriate error populations are produced and added to associated measurements, simulating errors from certain uncertainty sources. This produces large populations of perturbed measurements of all measurements taken during a test. Each set of perturbed measurements is then sent through the entire data reduction sequence to achieve thousands of simulated calculations of variables of interest. The perturbed populations of the variables of interest can then be analyzed to assess uncertainty in each variable.

The MCM was selected in lieu of the TSM due to the number of calculations involved and measurement uncertainty correlations present in the data reduction sequence. The method also lends itself well to quickly simulating theoretical changes for investigation of potential uncertainty improvements. For specific details on the methodology and application of both MCM and TSM, including examples of error population for uncorrelated and correlated uncertainties (Refs. [5] and [6]).

### 5.2.2 Elemental Standard Uncertainty Estimates

An elemental standard uncertainty is defined as “an estimate of the standard deviation of the parent population from which a particular elemental error originates.” (See the ISO *Guide to the Expression of Uncertainty in Measurement* (Ref. [7]), Coleman and Steele (Ref. [5]).) All elemental standard uncertainty estimates, sources, and quantities that serve as inputs into the error propagation are detailed in this section. Standard, 1-sigma uncertainty estimates are presented. Elemental standard uncertainty estimates

for measurement  $x$  will be denoted as  $b_x$  following standard nomenclature for systematic standard uncertainty categorization. Unless otherwise noted, a normal distribution of errors is assumed for elemental uncertainties propagated. Calibration cycles of all instruments involved in the data reduction are considered and accounted for within the simulations. The specific heat ratio for air,  $\gamma$ , as well as gas constants used in the data reduction scheme are assumed to have negligible uncertainty contributions.

Elemental uncertainties are estimated on a source-by-source basis. The Taylor Series Method (TSM) for uncertainty propagation is employed by MANTUS (“Measurement Analysis Tool for Uncertainty in Systems”) (Refs. [6] and [8]), an Excel® based tool that allows the user to break down the overall measurement into component parts, or modules, to easily handle the analysis of multilevel instrumentation systems. This captures instrument chain uncertainty contributions from the point of measurement through the data system output as depicted in Figure 10.

For the  $8 \times 6$  SWT MCM simulation, systematic uncertainty related to the accuracy of measurements and measurement systems was estimated using the MANTUS tool. Estimates for all critical measurements required to calculate the facility VOIs are listed in Table V. Unless otherwise stated, uncertainty estimates represent a standard uncertainty ( $1-\sigma$ ) value and are assumed to be characterized by a normal distribution.

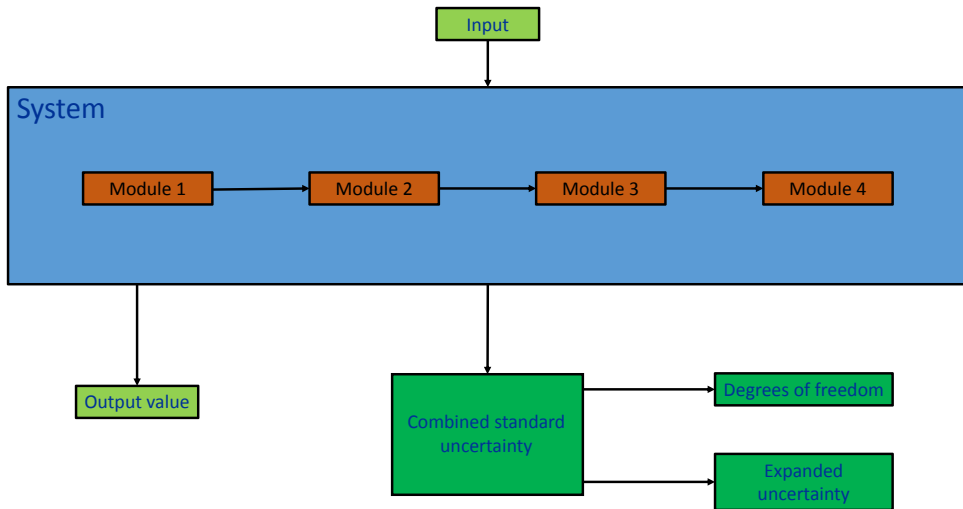


**Figure 10. Instrumentation level uncertainty analysis flow.**

**TABLE V. UNCERTAINTY ESTIMATES FOR CRITICAL MEASUREMENTS AND MEASUREMENT SYSTEMS**

Measurement system description	Label	Uncertainty estimate	Units
Mensor CPT 6180, 0-15 psia	Pbar	See Figure 11	psia
Optimus DTC, $\pm 15$ psid module	Optimus15psid	0.0045	psid
Temperature measured at reference junction, Kaye UTR/Fluke Black Stack	TCref	0.102	Rankine
Type E thermocouple with special limits of error wire	TC	See Figure 12	Rankine

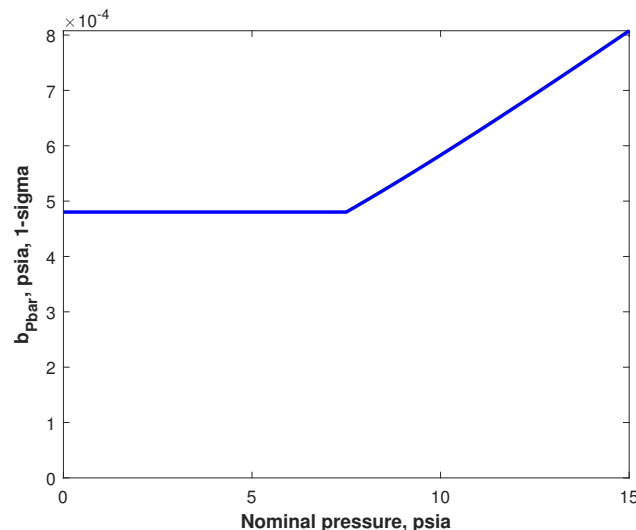


Figure 11. Elemental uncertainty estimates for Mensor CPT 6180, 0-15 psia pressure sensor.

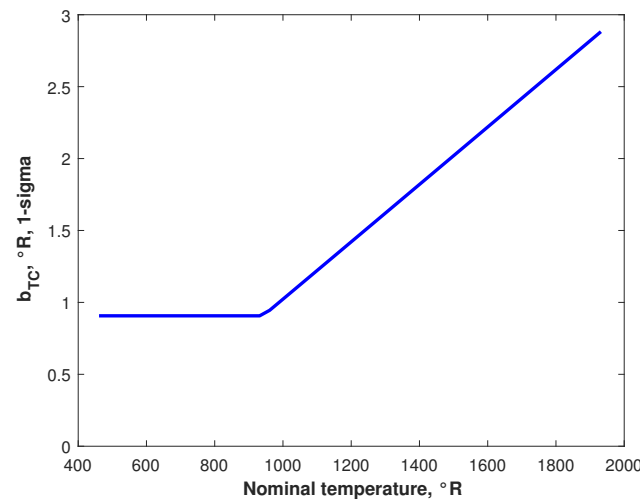


Figure 12. Elemental uncertainty estimates for Type E thermocouple with special limits of error wire.

### 5.2.3 Prediction Model Uncertainty Estimates

For any test-derived regression model, two uncertainty sources must be considered: the uncertainty fossilized into the model due to uncertainties present in the data obtained during the characterization test and the uncertainty due to the residual error of the model selected. The former of these is inherent in the results of the MCM because the characterization tests are included in the cascading simulation, the latter requires statistical analysis of the regression model residuals.

**Static Pressure Prediction Model Uncertainty.** Uncertainty estimates for the residual error of the static pressure prediction models were developed for scenarios 1, 2 and 3 described in Table II. Table VI shows the uncertainty estimates of the static pressure prediction models.

**Total Pressure Prediction Model Uncertainty.** Uncertainty estimates for the residual error of the total pressure prediction models were developed for cases 2 and 3 (Table II). Table VII shows the uncertainty estimates of the total pressure prediction models.

**Total Temperature Prediction Model Uncertainty.** Uncertainty estimates for residual error of the total temperature prediction models were developed for scenarios 2 and 3 (Table II). Table VIII shows the uncertainty estimates of the total temperature prediction models.

TABLE VI. STATIC PRESSURE PREDICTION MODEL UNCERTAINTY ESTIMATES

Flexwall Camshaft Angle	Nominal Mach	$u_{PScal,fit}$ Scenario 1 (On-nominal)	$u_{PScal,fit}$ Scenario 2 (Localized)	$u_{PScal,fit}$ Scenario 3 (Generalized)
48.1	1.1	0.00016	0.00075	—
67.6	1.2	0.00019	0.00075	—
80.3	1.3	0.00004	0.00040	—
101.3	1.4	0.00017	0.00100	—
121.3	1.5	0.00009	0.00030	—
138.8	1.6	0.00019	0.00026	—
154.3	1.7	0.00024	0.00031	—
167.7	1.8	0.00019	0.00028	—
180.0	1.9	0.00007	0.00022	—
190.4	2.0	0.00005	0.00017	—
Subsonic generalized	—	—	—	0.00011
Supersonic generalized	—	—	—	0.00075

TABLE VII. TOTAL PRESSURE PREDICTION MODEL UNCERTAINTY ESTIMATES

Flexwall Camshaft Angle	Nominal Mach	$u_{PTcal,fit}$ Scenario 2 (Localized)	$u_{PTcal,fit}$ Scenario 3 (Generalized)
48.1	1.1	0.00164	—
67.6	1.2	0.00008	—
80.3	1.3	0.00023	—
101.3	1.4	0.00025	—
121.3	1.5	0.00019	—
138.8	1.6	0.00004	—
154.3	1.7	0.00007	—
167.7	1.8	0.00010	—
180.0	1.9	0.00001	—
190.4	2.0	0.00011	—
Subsonic generalized	—	—	0.00001
Supersonic generalized	—	—	0.00164

TABLE VIII. TOTAL TEMPERATURE PREDICTION MODEL UNCERTAINTY ESTIMATES

Flexwall Camshaft Angle	Nominal Mach	$u_{TTcal,fit}$ Scenario 2 (Localized)	$u_{TTcal,fit}$ Scenario 3 (Generalized)
48.1	1.1	0.00020	—
67.6	1.2	0.00002	—
80.3	1.3	0.00007	—
101.3	1.4	0.00006	—
121.3	1.5	0.00013	—
138.8	1.6	0.00004	—
154.3	1.7	0.00007	—
167.7	1.8	0.00004	—
180.0	1.9	0.00001	—
190.4	2.0	0.00005	—
Subsonic generalized	—	—	0.00001
Supersonic generalized	—	—	0.00164

## 6 Data Reduction

Using test-time facility measurements and the calibrated values for  $P_{S,ts}$ ,  $P_{T,ts}$ , and  $P_{T,2,ts}$  as well as  $\gamma$  (the ratio of specific heats, assumed here to be a constant 1.4), the test section Mach number is calculated in the subsonic range by

$$M_{ts} = \sqrt{\frac{2}{\gamma - 1} \left[ \left( \frac{P_{S,ts}}{P_{T,ts}} \right)^{-\frac{\gamma-1}{\gamma}} - 1 \right]}, \quad (2)$$

and is solved for iteratively in the supersonic range using the Rayleigh Pitot formula using Equation 100 (Ref. [9]).

$$\frac{P_{T,2,ts}}{P_{S,ts}} = \left[ \frac{(\gamma + 1)M_{ts}^2}{2} \right]^{\frac{\gamma}{\gamma-1}} \left[ \frac{\gamma + 1}{2\gamma M_{ts}^2 - (\gamma - 1)} \right]^{\frac{1}{\gamma-1}}. \quad (3)$$

The data flow from measured values to Mach number is presented in Figure 13 for subsonic flow, and in Figure 14 for supersonic flow. The supersonic test section total pressure can then be calculated using Equation 99 (Ref. [9]).

$$\frac{P_{T,2,ts}}{P_{T,ts}} = \left[ \frac{(\gamma + 1)M_{ts}^2}{(\gamma - 1)M_{ts}^2 + 2} \right]^{\frac{\gamma}{\gamma-1}} \left[ \frac{\gamma + 1}{2\gamma M_{ts}^2 - (\gamma - 1)} \right]^{\frac{1}{\gamma-1}}. \quad (4)$$

Test section static temperature is defined as

$$T_{S,ts} = \frac{T_{T,ts}}{1 + \frac{\gamma-1}{2} M_{ts}^2}. \quad (5)$$

Test section free stream airspeed is defined as

$$U_{ts} = M_{ts} \sqrt{\gamma \cdot R \cdot T_{S,ts}}. \quad (6)$$

Test section air density is calculated as

$$\rho_{ts} = \frac{P_{S,ts}}{R \cdot T_{S,ts}}, \quad (7)$$

and test section air viscosity (slugs/(ft · sec)) is

$$\mu_{ts} = 2.270 \frac{T_{S,ts}^{1.5}}{T_{S,ts} + 198.6} \cdot 10^{-8} \quad (8)$$

for  $T_{S,ts}$  in  ${}^{\circ}R$ . Test section Reynolds number per unit length is calculated as

$$Re_{ts} = \frac{\rho_{ts} U_{ts}}{\mu_{ts}}, \quad (9)$$

and the test section dynamic pressure is

$$q_{ts} = P_{T,ts} \cdot \frac{\gamma}{2} M_{ts}^2 \left( 1 + \frac{\gamma - 1}{2} M_{ts}^2 \right)^{-\frac{\gamma}{\gamma-1}}. \quad (10)$$

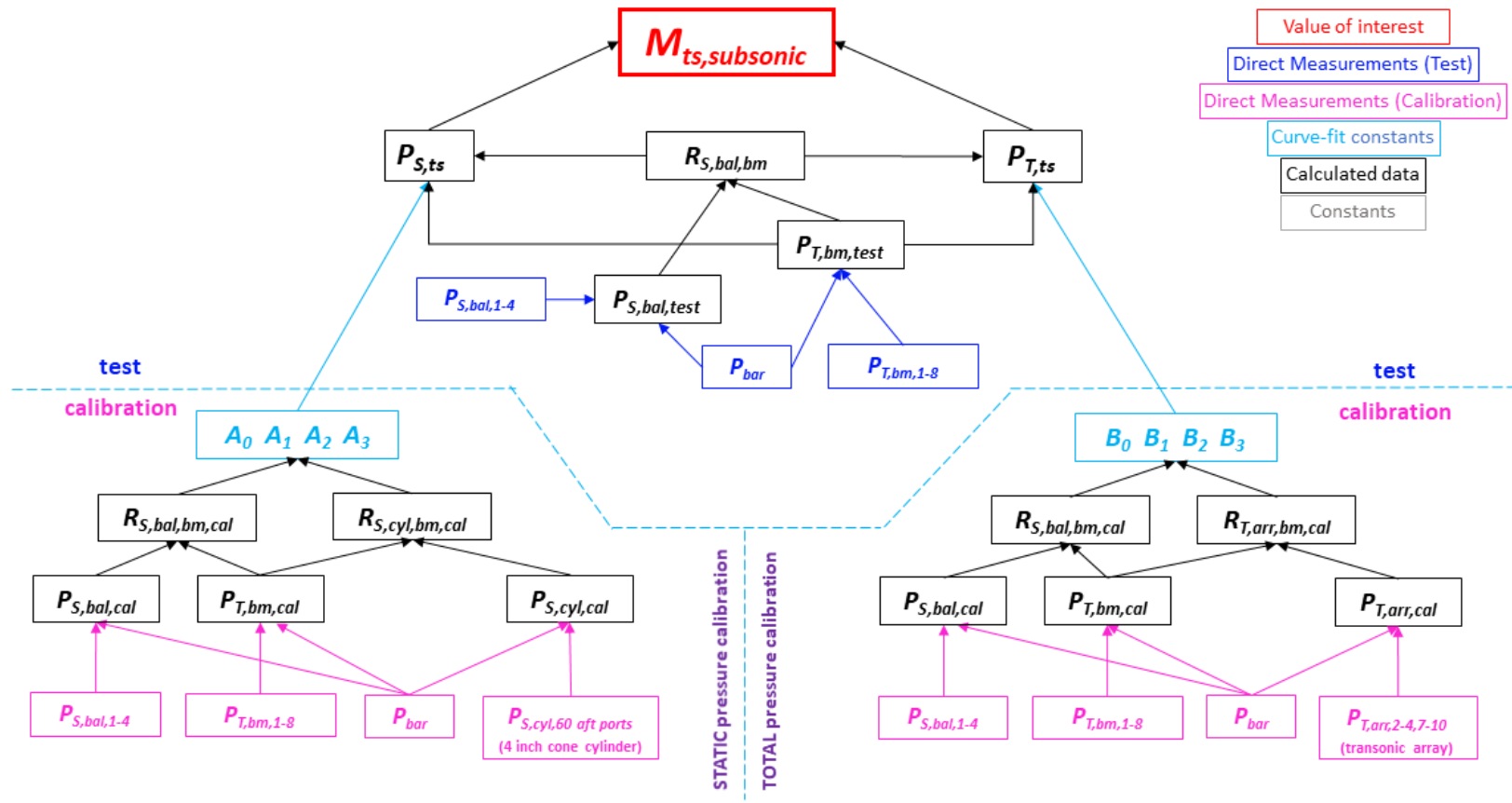


Figure 13. Data flow from measured value to calculated Mach number for subsonic flow.

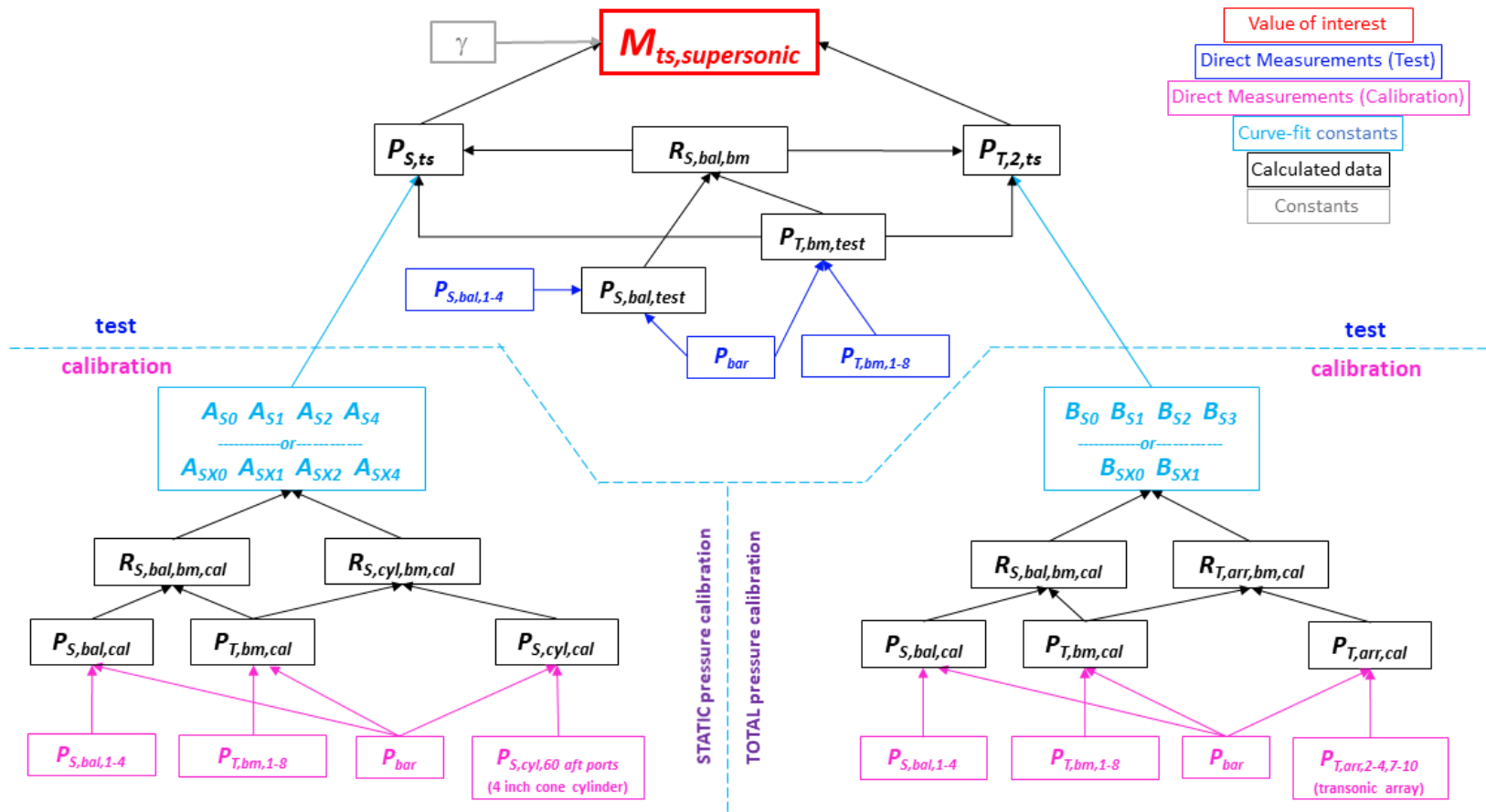


Figure 14. Data flow from measured value to calculated Mach number for supersonic flow.

## 7 Results

The results presented here are from the  $8 \times 6$  SWT uncertainty analysis of test section porosity configuration 1. Results are presented as expanded uncertainties, with a coverage factor of  $k = 2$ , which is approximately equal to a level of confidence of 95 percent. The expanded uncertainties are denoted by  $S_x$ ,  $B_x$ , and  $U_x$  for random, systematic and combined uncertainty, respectively. Each VOI is treated as univariate. Uncertainty Percent Contribution (UPC) charts, which show the primary factors contributing to the overall uncertainty in a VOI and the percentage that each factor contributes, are presented for the systematic uncertainty of the calculated VOIs.

For the  $8 \times 6$  SWT, it is difficult to separate truly random variation in pressure measurements from allowed operational variation to accurately characterize random uncertainty in measured pressures. To further explain, an overview of typical facility operation is given below.

The  $8 \times 6$  SWT is designed to achieve and hold a desired test section Mach number for the purpose of observing test article response. Operationally, test section Mach number is a function of four components:

1. Flexwall setting, which adjusts the contour of the tunnel's convergent-divergent nozzle to the area ratio of the nozzle throat to nozzle exit for the specified setpoint.
2. Compressor drive speed, which determines plenum total pressure at the specified setpoint. Other than setting the drive speed, the plenum total pressure is not controlled. Within the timeframe of a test point, the total pressure at a particular drive speed is typically constant; however, it can vary between repeat test points taken at different times.
3. Balance chamber exhaust valve position, which adjusts the balance chamber static pressure to control the static to total pressure ratio required to achieve the specified Mach number and optimal flow quality at nominal setpoints.
4. Position of shock doors.

Once on setpoint, the flexwall setpoint and compressor drive speed are essentially constant. The balance chamber static pressure varies, as needed, to maintain the pressure ratio to stay on point. As such, the pressure ratio is the critical variable in controlling test section Mach number rather than the individual values of total and static pressure. Higher variation might be seen in the pressure measurements from repeat to repeat, but the random variation in the pressure ratio, and therefore in Mach number, remains very low. However the variability in pressure measurements may affect the uncertainty of other calculated VOIs that use the pressure measurements directly, rather than the pressure ratio, in the calculations. The shock doors are only used in subsonic operation. They are brought into the flow to back pressure the compressor at low subsonic speeds. The doors are always flush at supersonic conditions. The aft-to-balance chamber pressure ratio is not included in the calibration, but is another facility control variable that might be of interest if unusually high variation is observed at subsonic conditions.

The results presented here include the characterization of random and systematic effects from instrumentation, prediction models, and observed variation on Mach number. In addition, systematic uncertainty characterization results are presented for other calculated VOIs.

A detailed description of the test matrix is included in Section 4.2 of the 2019 characterization test report (Ref. [1]).

### 7.1 Mach Number Uncertainty

#### 7.1.1 Repeatability (Random) Uncertainty Characterization

As described in Section 5.1, repeatability uncertainty characterizes the variation of a measurement about its mean. This type of uncertainty may be of interest to researchers looking for small changes due to model modifications. These results provide an understanding of the facility's within-test variation.

Figure 15 shows a plot of random uncertainty in Mach number over the subsonic and supersonic operating ranges of the  $8 \times 6$  SWT. The random uncertainty in Mach number is very low, i.e., less than 0.00004 throughout the operating range. Table IX summarizes the random uncertainty in Mach number.

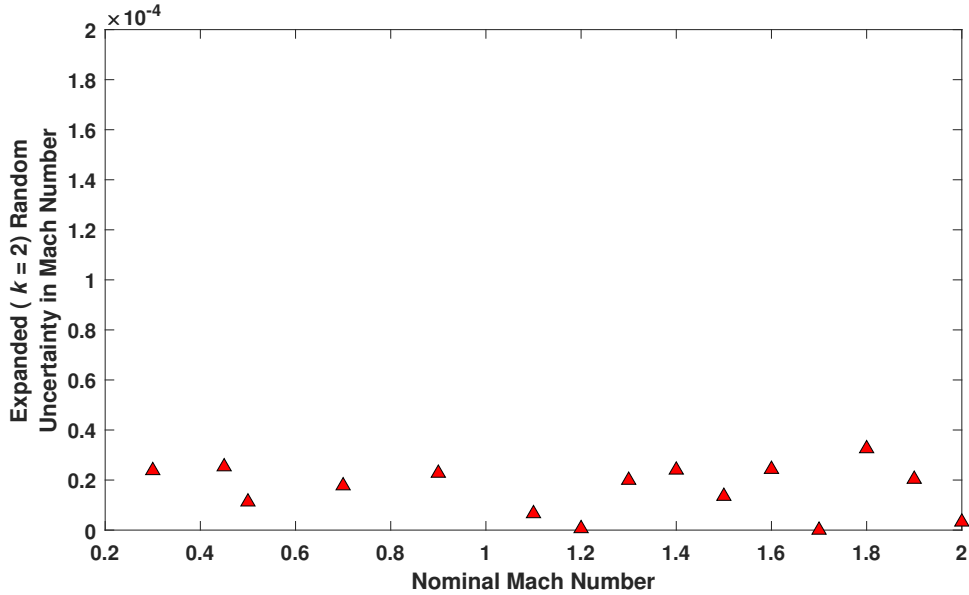


Figure 15. Random uncertainty in  $M_{ts}$  as a function of nominal Mach number for test section porosity configuration 1.

TABLE IX. SUMMARY OF RANDOM UNCERTAINTY RESULTS FOR CALCULATED TEST SECTION MACH NUMBER, TEST SECTION POROSITY CONFIGURATION 1

Nominal Mach	Typical $M_{ts}$	$S_{M_{ts}}$ $k=2$
0.30	0.30	0.000024
0.45	0.40	0.000025
0.50	0.50	0.000011
0.70	0.70	0.000018
0.90	0.90	0.000023
1.20	1.18	0.000001
1.40	1.35	0.000024
1.60	1.56	0.000024
1.80	1.78	0.000033
2.00	2.00	0.000003

### 7.1.2 Systematic Uncertainty Characterization

The uncertainty results presented in this section are a characterization of the effects of the systematic error due to measurement process, instrumentation calibrations and measurements, installation effects and other similar sources that introduce bias on Mach number.

Figure 16 shows  $B_{M,ts}$  over the nominal operating range of the facility, using the generalized curve fit prediction models (generalized) for subsonic and supersonic operations.  $B_{M,ts}$  decreases from 0.002 to 0.001 between M 0.25 and M 0.4 and then remains constant at 0.001 from M 0.4 through M 1.0.  $B_{M,ts}$  increases in the supersonic range (M 1.1 to M 2.0) from 0.004 to 0.014.

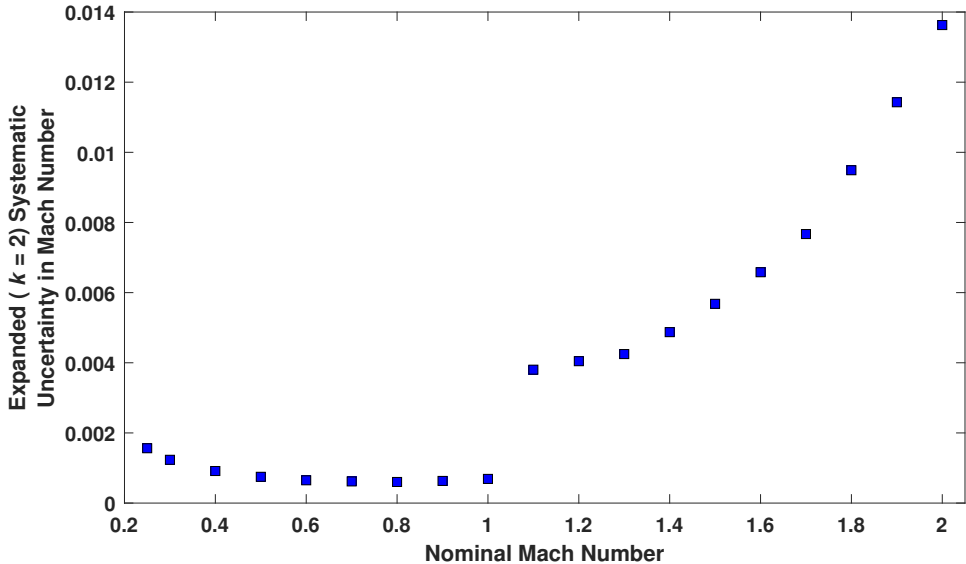


Figure 16. Systematic uncertainty in  $M_{ts}$  as a function of nominal Mach number for test section porosity configuration 1.

Figure 17 shows a comparison of  $B_{M,ts}$  over the supersonic operating range, for the prediction model scenarios defined in Table II.

In scenario 1, when flexwall position and  $R_{S,bal,bm}$  are within on-nominal limits, localized prediction models, with an additional correction factor added to the  $P_{S,ts}$  prediction, are used to calculate  $M_{ts}$ . For scenario 2, when flexwall position and  $R_{S,bal,bm}$  are within localized limits, but  $R_{S,bal,bm}$  is not within on-nominal limits,  $M_{ts}$  is calculated using localized prediction models without the static pressure correction factor. When both flexwall position and  $R_{S,bal,bm}$  are outside of localized limits, the generalized prediction model is used to calculate  $M_{ts}$ .

For scenario 2, there were not enough seed data points at M 1.1 and M 1.2 to perform a statistical analysis to calculate a valid prediction model uncertainty estimate. In those cases, the prediction model uncertainty estimates for scenario 3 (fully off-nominal) were used for error propagation.

$B_{M_{ts}}$  is at its lowest for scenario 1, remaining at or below 0.003 throughout the supersonic operating range. In scenario 2,  $B_{M_{ts}}$  increases slightly, but remains less than 0.004 throughout the supersonic range, with an exception at M 1.4. In scenario 3,  $B_{M_{ts}}$  follows the generalized curve fit prediction model shown in Figure 16.

Figures 18, 19 and 20 show the percent contributions of the primary contributors to uncertainty in the calculation of  $M_{ts}$  for scenarios 3, 2 and 1, respectively.

Scenario 3 (Figure 18) is the worst-case scenario. In this case, a number of factors contribute significantly to the uncertainty in Mach number in the subsonic range. These include the live measurements of static and total pressures during testing (PTBM, and PSBAL), the static and total pressure calibration processes (PSCAL and PT\_TTcal), and the prediction model error of the static pressure calibration models. In the supersonic range, the prediction model error for both the static and total pressure calibration models are the dominant contributors to uncertainty in  $M_{ts}$ . At M 1.1, they contribute equally to  $B_{M_{ts}}$ . As Mach number increases, the static pressure prediction model error gradually becomes the predominant contributor to  $B_{M_{ts}}$ .

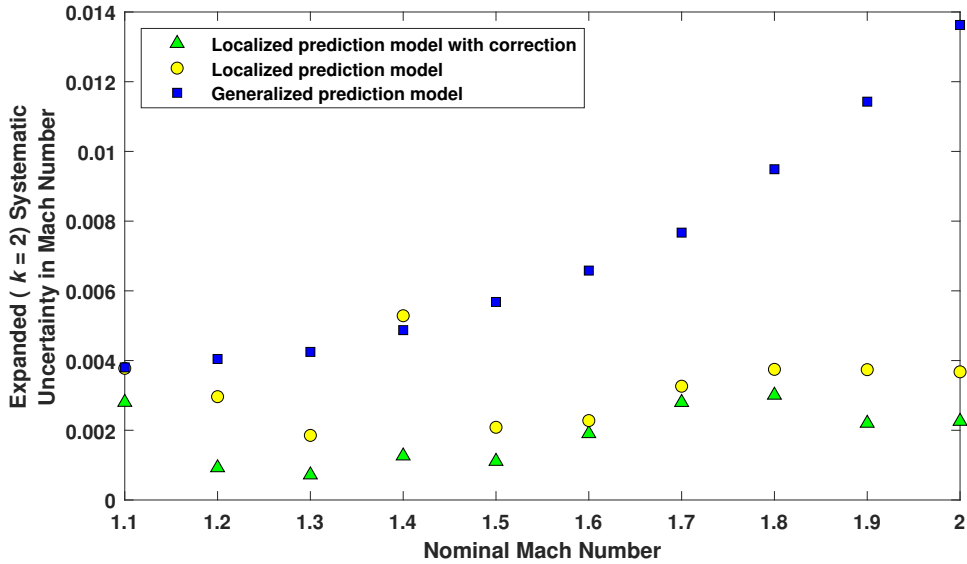


Figure 17. Comparison of systematic uncertainty in  $M_{ts}$  for prediction model scenarios 1, 2 and 3 (Table II), as a function of nominal Mach number for test section porosity configuration 1.

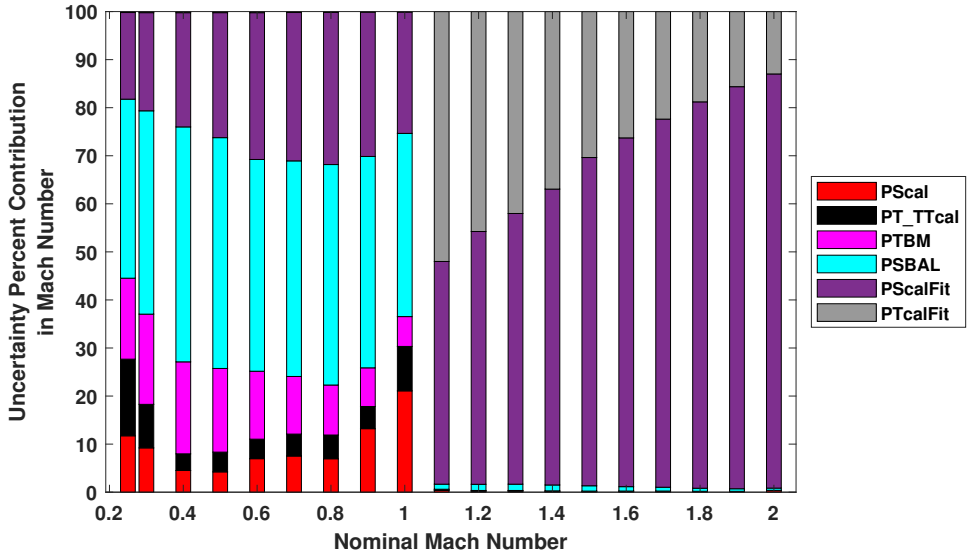
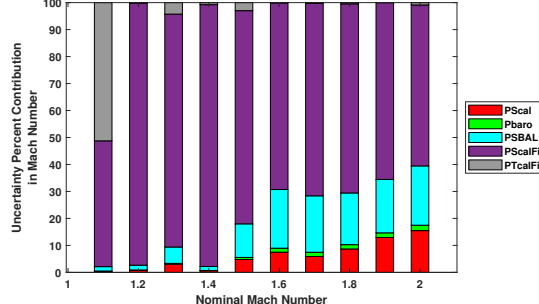


Figure 18. Systematic UPC of  $M_{ts}$  as a function of nominal Mach number for scenario 3, test section porosity configuration 1.

In scenario 2 (Figure 19), the contribution of the total pressure prediction model error to  $B_{M_{ts}}$  is reduced significantly. The static pressure prediction model error remains the dominant contributor, but it is reduced somewhat. As Mach number increases, the balance chamber static pressure measurements and the static pressure calibration process begin to introduce significant contributions.

In scenario 1 (Figure 20) initially, the static and total pressure prediction model errors are the dominant contributors to  $B_{M_{ts}}$ . As Mach number increases, the static pressure prediction model error and live pressure measurements become the dominant contributors. The static pressure calibration process also introduces a consistent contribution over the supersonic operation range.

Table X summarizes the results of the Monte Carlo simulation for the calculation of  $M_{ts}$  for scenario 3.



**Figure 19.** Systematic UPC of  $M_{ts}$  as a function of nominal Mach number for scenario 2, test section porosity configuration 1.

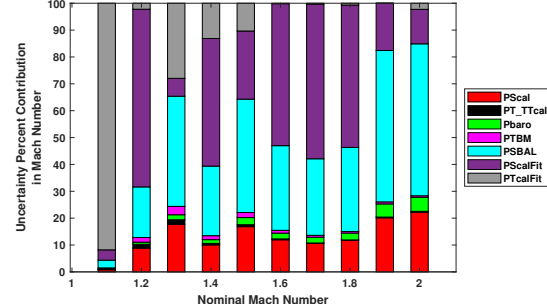


**Figure 20.** Systematic UPC of  $M_{ts}$  as a function of nominal Mach number for scenario 1, test section porosity configuration 1.

**TABLE X. SUMMARY OF SYSTEMATIC UNCERTAINTY RESULTS FOR CALCULATED MACH NUMBER, SCENARIO 3, TEST SECTION POROSITY CONFIGURATION 1**

Nominal Mach	Typical $M_{ts}$	$B_{M_{ts}}$ $k=2$	$B_{M_{ts}}$ UPC due to $b_{P_{S,cal}}$	$B_{M_{ts}}$ UPC due to $b_{P_T-T_{T,cal}}$	$B_{M_{ts}}$ UPC due to $b_{P_{T,bm}}$	$B_{M_{ts}}$ UPC due to $b_{P_{T,bm}}$	$B_{M_{ts}}$ UPC due to $b_{P_{Scal,fit}}$	$B_{M_{ts}}$ UPC due to $b_{P_{Tcal,fit}}$
0.25	0.25	0.0016	11.7	15.9	16.8	37.2	18.0	0.2
0.40	0.40	0.0009	4.5	3.5	19.1	48.9	23.8	0.2
0.60	0.60	0.0006	7.0	4.1	14.1	44.1	30.5	0.2
0.80	0.80	0.0006	7.0	4.9	10.4	45.9	31.7	0.2
1.00	0.95	0.0007	21.1	9.2	6.2	38.1	25.3	0.1
1.20	1.18	0.0040	0.2	0.0	0.1	1.3	52.6	45.8
1.40	1.35	0.0049	0.2	0.0	0.1	1.2	61.6	36.9
1.60	1.56	0.0066	0.2	0.0	0.0	0.9	72.6	26.3
1.80	1.78	0.0095	0.1	0.0	0.0	0.6	80.4	18.8
2.00	2.00	0.0136	0.3	0.1	0.0	0.5	86.2	13.0

### 7.1.3 Combined Uncertainty Characterization

Combined uncertainty characterization results for Mach number are presented in Figure 21. The combined uncertainty is essentially equal to the systematic uncertainty because the random uncertainty is very small relative to the systematic uncertainty. Table XI summarizes the random, systematic and combined uncertainty in Mach number.

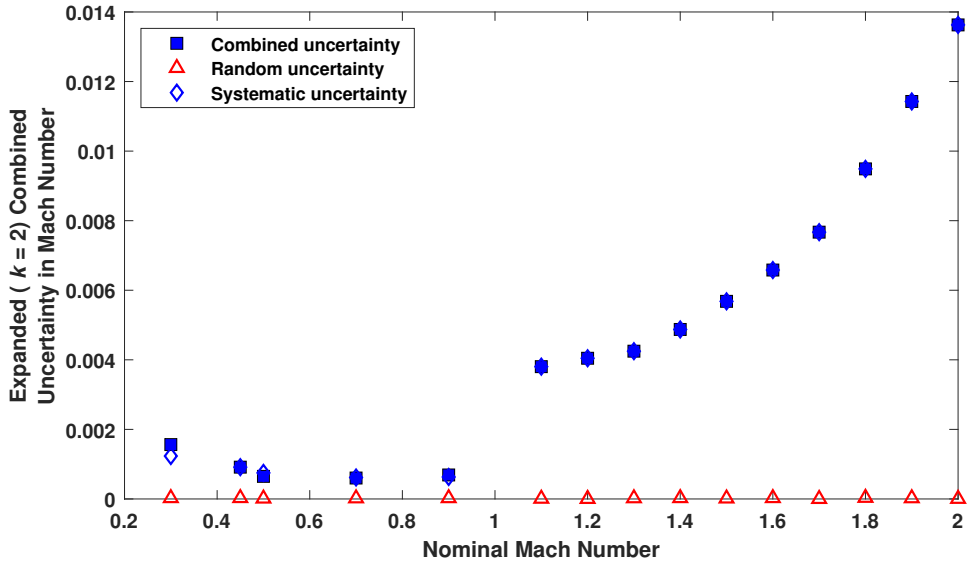


Figure 21. Combined uncertainty in  $M_{ts}$  as a function of nominal Mach number for test section porosity configuration 1.

TABLE XI. SUMMARY OF RANDOM, SYSTEMATIC AND COMBINED UNCERTAINTY RESULTS FOR CALCULATED MACH NUMBER, SCENARIO 3, TEST SECTION POROSITY CONFIGURATION 1

Nominal Mach	Typical $M_{ts}$	$S_{M_{ts}}$ $k=2$	$B_{M_{ts}}$ $k=2$	$U_{M_{ts}}$ $k=2$
0.30	0.30	0.000024	0.0012	0.0012
0.40	0.40	0.000025	0.0009	0.0009
0.50	0.50	0.000011	0.0007	0.0007
0.70	0.70	0.000018	0.0006	0.0006
0.90	0.90	0.000023	0.0006	0.0006
1.20	1.18	0.000001	0.0040	0.0040
1.40	1.35	0.000024	0.0049	0.0049
1.60	1.56	0.000024	0.0066	0.0066
1.80	1.78	0.000033	0.0095	0.0095
2.00	2.00	0.000003	0.0136	0.0136

## 7.2 Systematic Uncertainty Results for Other VOIs

The uncertainty results presented in this section are a characterization of the effects of the systematic error due to measurement process, instrumentation calibrations and measurements, installation effects and other similar sources that introduce bias on static pressure, total pressure, dynamic pressure, total temperature, static temperature, air speed, and Reynolds number.

### 7.2.1 Static Pressure Systematic Uncertainty

Figure 22 shows  $B_{P_{S,ts}}$  over the nominal operating range of the facility, using the generalized curve fit prediction models (scenario 3) for subsonic and supersonic operations.  $B_{P_{S,ts}}$  is approximately 0.007 psi over the entire subsonic range and increases from 0.03 psi to 0.4 psi over the supersonic range.

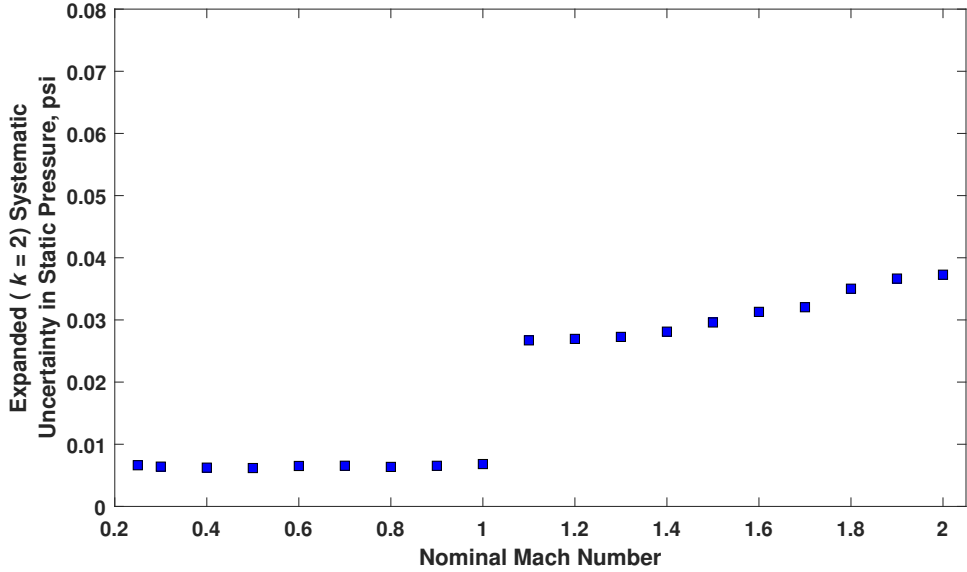


Figure 22. Systematic uncertainty in  $P_{S,ts}$  as a function of nominal Mach number for test section porosity configuration 1.

Figure 23 shows a comparison of  $B_{P_{S,ts}}$  over the supersonic operating range, for the prediction model scenarios defined in Table II.

In scenario 1, when flexwall position and  $R_{S,bal,bm}$  are within on-nominal limits,  $P_{S,ts}$  is calculated using localized prediction models, with an additional correction factor added to the calculation.  $B_{P_{S,ts}}$  is at its lowest for this scenario, remaining at or below approximately 0.01 psi throughout the supersonic operating range.

For scenario 2, when flexwall position and  $R_{S,bal,bm}$  are within localized limits but  $R_{S,bal,bm}$  is not within on-nominal limits,  $P_{S,ts}$  is calculated using localized prediction models, without the additional correction factor. At M 1.1 and M 1.2, there were not enough seed data points to perform a statistical analysis to calculate a valid prediction model uncertainty estimate. In those cases, the prediction model uncertainty estimates for scenario 3 (fully off-nominal) were used for error propagation. In scenario 2,  $B_{P_{S,ts}}$  increases but remains less than 0.02 psi throughout the supersonic range, with an exception at M 1.4. This exception is a reflection of unusually high variability at the M 1.4 setpoint in the Monte Carlo simulation seed data extracted from the 2019 characterization test (Ref. [1]) data. Further investigation at this setpoint is recommended in future characterization tests. For scenario 3, when flexwall position and  $R_{S,bal,bm}$  fall outside of localized limits,  $B_{P_{S,ts}}$  follows the generalized curve fit prediction model shown in Figure 22.

Figures 24, 25 and 26 show the percent contributions of the primary contributors to uncertainty in the calculation of  $P_{S,ts}$  for scenarios 3, 2 and 1, respectively.

In scenario 3 (Figure 24), the live measurement of static pressures during testing is the biggest contributor to  $B_{P_{S,ts}}$  in the subsonic range. The second largest contributor to  $B_{P_{S,ts}}$  is the static pressure prediction model error. The static pressure calibration process and measurement of barometric pressure are also significant contributors to  $B_{P_{S,ts}}$ . In the supersonic range, the static pressure prediction model error is the dominant contributor to  $B_{P_{S,ts}}$ .

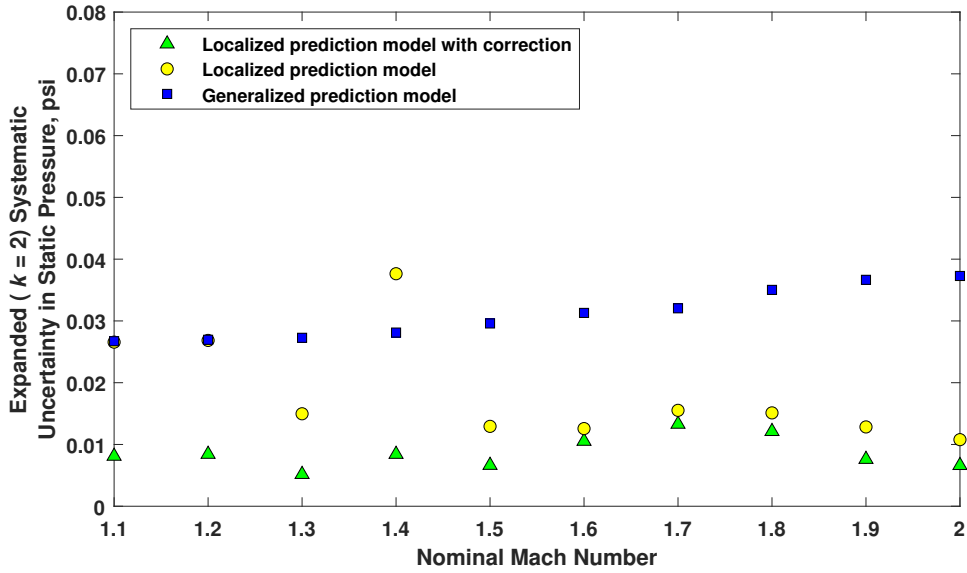


Figure 23. Comparison of systematic uncertainty in  $P_{S,ts}$  for prediction model scenarios 1, 2 and 3 (Table II), as a function of nominal Mach number for test section porosity configuration 1.

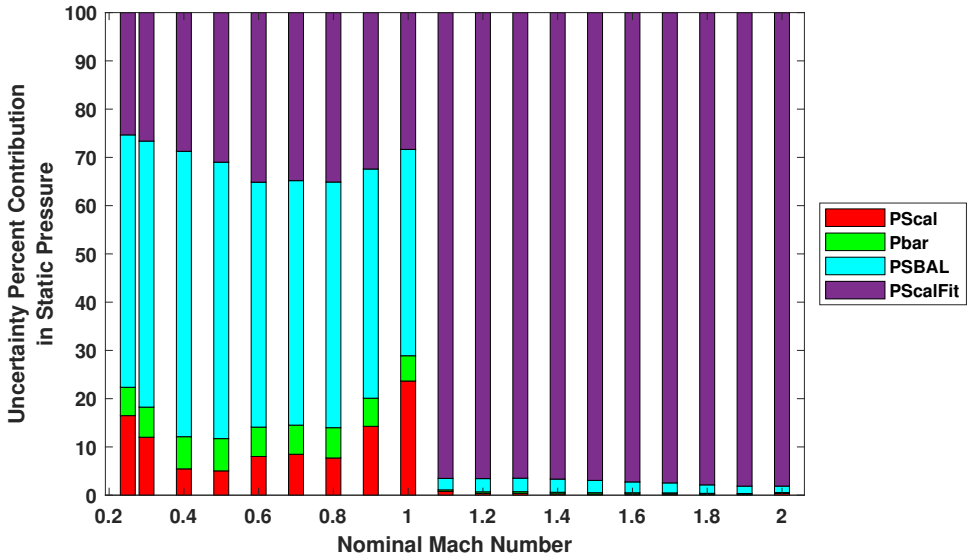


Figure 24. Systematic UPC of  $P_{S,ts}$  as a function of nominal Mach number for test section porosity configuration 1.

In scenario 2 (Figure 25), as Mach number increases, the contribution of the static pressure prediction model error reduces somewhat. The static pressure measurements and the static pressure calibration process have increasing contributions to  $B_{P_{S,ts}}$  as Mach number increases.

In scenario 1 (Figure 26), the contribution of the static prediction model error to  $B_{P_{S,ts}}$  is further reduced. The contributions from the pressure measurements are larger throughout the supersonic operating range as are the contributions from the static pressure calibration process.

Table XII summarizes the results of the Monte Carlo simulation for the calculation of  $P_{S,ts}$ .

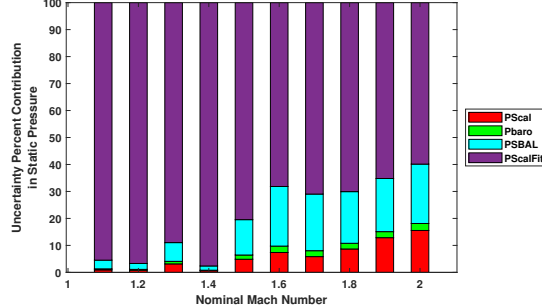


Figure 25. Systematic UPC of  $P_{S,ts}$  as a function of nominal Mach number for scenario 2, test section porosity configuration 1.

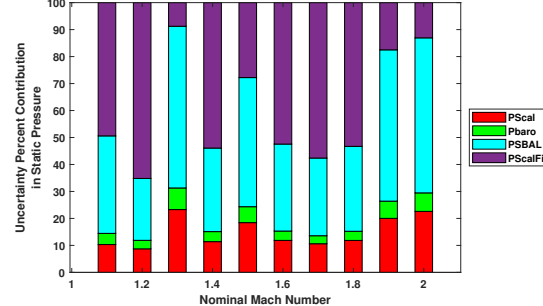


Figure 26. Systematic UPC of  $P_{S,ts}$  as a function of nominal Mach number for scenario 1, test section porosity configuration 1.

TABLE XII. SUMMARY OF SYSTEMATIC UNCERTAINTY RESULTS FOR CALCULATED TEST SECTION STATIC PRESSURE, SCENARIO 3, TEST SECTION POROSITY CONFIGURATION 1

Nominal Mach	Typical $P_{S,ts}$ psia	$B_{P_{S,ts}}$ psia $k=2$	$B_{P_{S,ts}}$ UPC due to $b_{P_{S,cal}}$	$B_{P_{S,ts}}$ UPC due to $b_{P_{bar}}$	$B_{P_{S,ts}}$ UPC due to $b_{P_{S,bal}}$	$B_{P_{S,ts}}$ UPC due to $b_{P_{S,fit}}$
0.25	14.64	0.0066	16.5	5.9	52.3	25.3
0.40	13.71	0.0062	5.5	6.7	59.1	28.7
0.60	13.78	0.0065	8.0	6.1	50.8	35.1
0.80	11.32	0.0064	7.7	6.3	50.9	35.1
1.00	9.36	0.0068	23.7	5.2	42.8	28.3
1.20	7.48	0.0269	0.4	0.3	2.7	96.6
1.40	6.16	0.0281	0.3	0.3	2.7	96.7
1.60	5.06	0.0313	0.2	0.3	2.2	97.3
1.80	4.12	0.0350	0.2	0.2	1.8	97.9
2.00	3.23	0.0373	0.4	0.2	1.3	98.1

### 7.2.2 Total Pressure Systematic Uncertainty

Figure 27 shows  $B_{P_{T,ts}}$  over the nominal operating range of the facility, using the generalized curve fit prediction models (scenario 3) for subsonic and supersonic operations.  $B_{P_{T,ts}}$  is approximately 0.004 psia over the subsonic range. In the supersonic range,  $B_{P_{T,ts}}$  increases, nonlinearly, from 0.06 psia to 0.3 psia.

Figure 28 shows a comparison of  $B_{P_{T,ts}}$  over the supersonic operating range, for the prediction model scenarios defined in Table II. In scenario 1, when flexwall position and  $R_{S,bal,bm}$  are within on-nominal limits,  $P_{T,ts}$  is calculated using localized prediction models, with an additional correction factor added to the calculation of  $P_{S,ts}$ . For scenario 2, when flexwall position and  $R_{S,bal,bm}$  are within localized limits but  $R_{S,bal,bm}$  falls outside of on-nominal limits,  $P_{T,ts}$  is calculated using localized prediction models without the static pressure correction factor. For scenarios 1 and 2,  $B_{P_{T,ts}}$  is essentially the same from M 1.1 to M1.7. As Mach number increases above M 1.7  $B_{P_{T,ts}}$  is slightly higher for scenario 2.  $B_{P_{T,ts}}$  ranges from 0.01 psia to about 0.06 psia. For scenario 3, when flexwall position and  $R_{S,bal,bm}$  fall outside of localized limits,  $P_{T,ts}$  is calculated using the generalized prediction model and  $B_{P_{T,ts}}$  ranges from 0.06 psia to 0.3 psia.

Figures 29, 30 and 31 show the percent contributions of the primary contributors to uncertainty in the calculation of  $P_{T,ts}$  for scenarios 3, 2 and 1, respectively.

In scenario 3 (Figure 29), the live measurement of total pressures during testing is the biggest contributor to  $B_{P_{T,ts}}$  in the subsonic range. The total pressure calibration process and measurement of barometric pressure are also significant contributors. In the supersonic range, the dominant contributor to  $B_{P_{T,ts}}$  is the total pressure prediction model error. As Mach number increases, the static pressure prediction model error also contributes to  $B_{P_{T,ts}}$ .

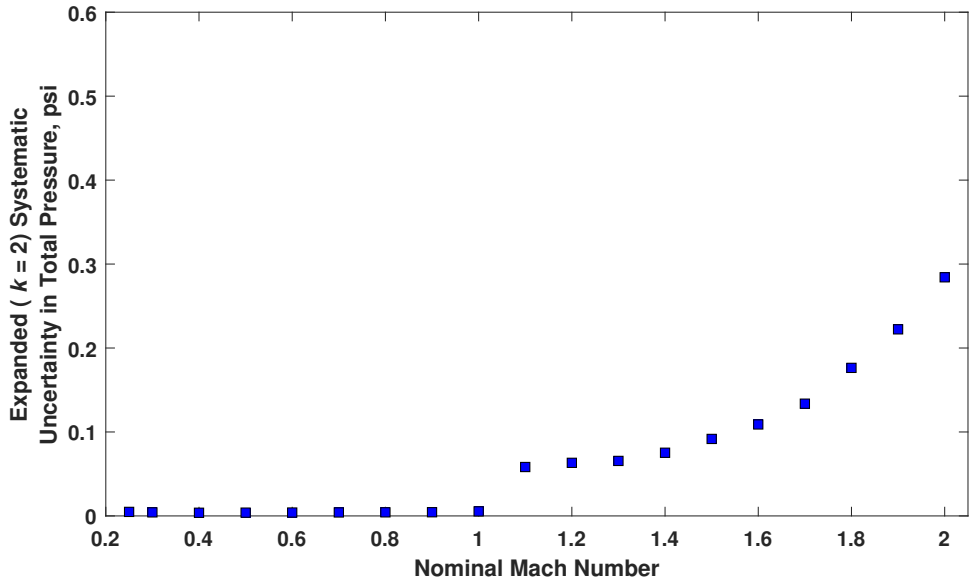


Figure 27. Systematic uncertainty in  $P_{T,ts}$  as a function of nominal Mach number for test section porosity configuration 1.

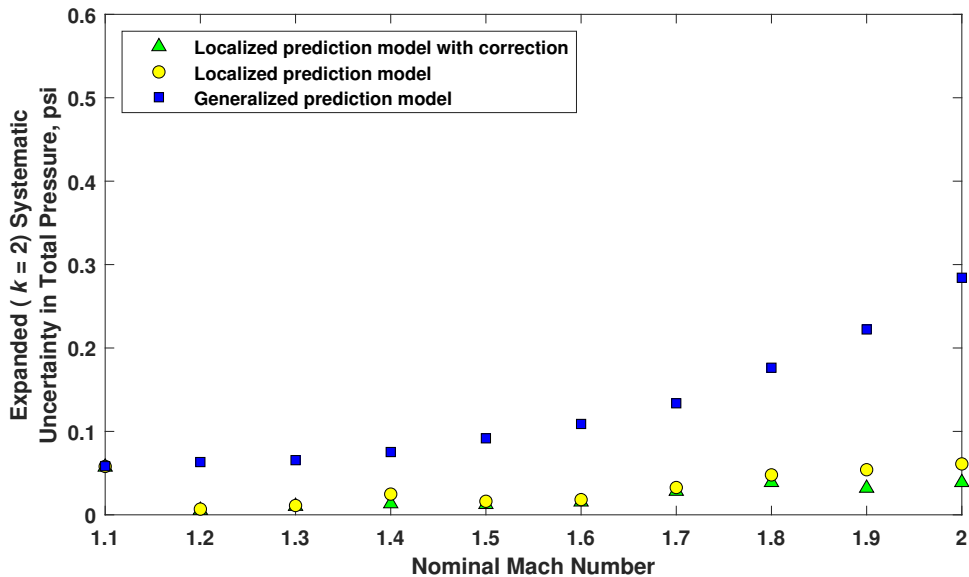


Figure 28. Comparison of systematic uncertainty in  $P_{T,ts}$  for prediction model scenarios 2 and 3 (Table II), as a function of nominal Mach number for test section porosity configuration 1.

In scenario 2 (Figure 30), at M 1.1, the error from the total pressure prediction model is the main contributor to  $B_{P_{T,ts}}$ . As Mach number increases, uncertainty introduced from the static pressure prediction model error increases in significance. Measurement of static pressures and the static pressure calibration process also have significant contributions.

In scenario 1 (Figure 31) between M 1.1 and M 1.5, the total pressure prediction model error is the largest contributor to  $B_{P_{T,ts}}$ . As Mach number increases within that range, contributions from the total pressure measurements and the total pressure calibration process become significant. Above M 1.5, the main contributions to  $B_{P_{T,ts}}$  are from the static pressure prediction model error, static pressure measurements, and the static pressure calibration process.

Table XIII summarizes the results of the Monte Carlo simulation for the calculation of  $P_{T,ts}$ .

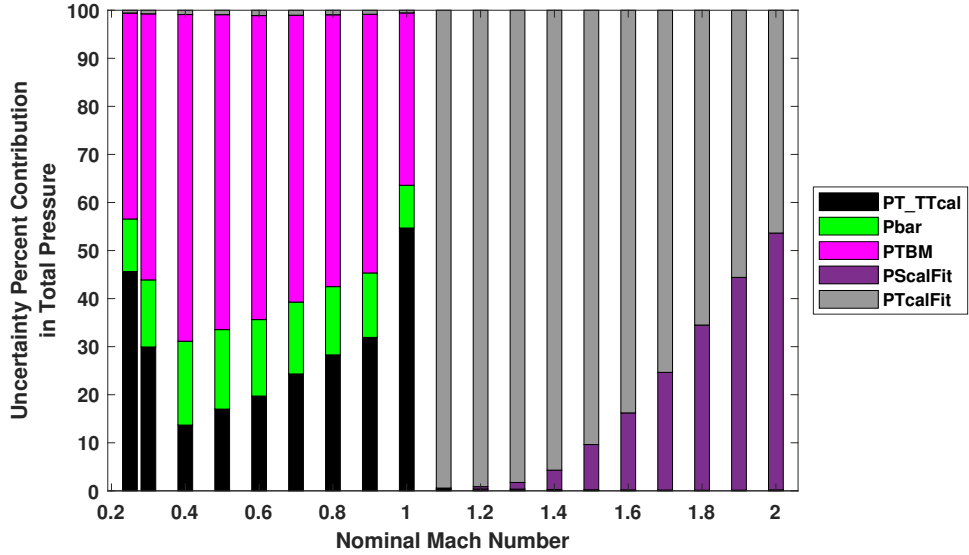


Figure 29. Systematic UPC of  $P_{T,ts}$  as a function of nominal Mach number for scenario 3, test section porosity configuration 1.

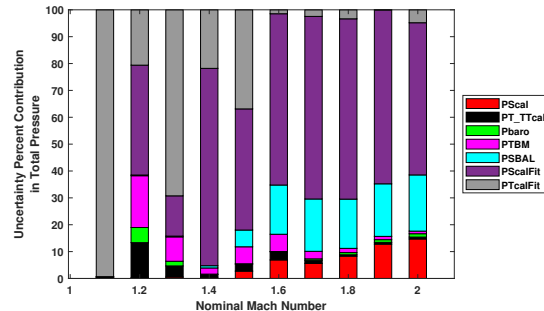


Figure 30. Systematic UPC of  $P_{T,ts}$  as a function of nominal Mach number for scenario 2, test section porosity configuration 1.

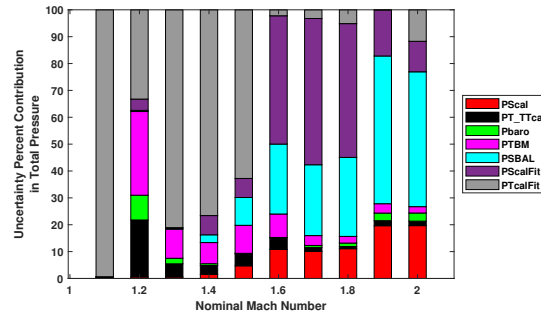


Figure 31. Systematic UPC of  $P_{T,ts}$  as a function of nominal Mach number for scenario 1, test section porosity configuration 1.

TABLE XIII. SUMMARY OF SYSTEMATIC UNCERTAINTY RESULTS FOR CALCULATED TEST SECTION TOTAL PRESSURE, SCENARIO 3, TEST SECTION POROSITY CONFIGURATION 1

Nominal Mach	Typical $P_{T,ts}$ psia	$B_{P_{T,ts}}$ psia $k=2$	$B_{P_{T,ts}}$ UPC due to $b_{P_T-T_{T,cal}}$	$B_{P_{T,ts}}$ UPC due to $b_{P_{bar}}$	$B_{P_{T,ts}}$ UPC due to $b_{P_{T,bm}}$	$B_{P_{T,ts}}$ UPC due to $b_{P_{S,fit}}$	$B_{P_{T,ts}}$ UPC due to $b_{P_{T,fit}}$
0.25	15.30	0.0048	45.6	10.9	42.9	0.0	0.6
0.40	15.32	0.0038	13.7	17.4	68.0	0.0	0.9
0.60	17.57	0.0040	19.7	15.9	63.3	0.0	1.1
0.80	17.26	0.0043	28.3	14.2	56.6	0.0	0.9
1.00	16.74	0.0054	54.7	8.9	35.9	0.0	0.5
1.20	17.74	0.0633	0.1	0.1	0.3	0.5	99.1
1.40	18.33	0.0753	0.1	0.0	0.2	4.0	95.7
1.60	20.26	0.1089	0.1	0.0	0.1	16.0	83.8
1.80	22.95	0.1764	0.1	0.0	0.0	34.4	65.5
2.00	25.24	0.2842	0.2	0.0	0.0	53.4	46.4

### 7.2.3 Dynamic Pressure Systematic Uncertainty

Figure 32 shows  $B_{Q_{ts}}$  over the nominal operating range of the facility, using the generalized curve fit prediction models (scenario 3) for subsonic and supersonic operations.  $B_{Q_{ts}}$  ranges from 0.005 psia to 0.008 psia in the subsonic range. In the supersonic range,  $B_{Q_{ts}}$  ranges from 0.034 psia to 0.046 psia.

Figures 33, 34 and 35 show the percent contributions of the primary contributors to uncertainty in the calculation of  $Q_{ts}$  for scenarios 3, 2 and 1, respectively.

In scenario 3 (Figure 33), a number of factors contribute significantly to  $B_{Q_{ts}}$  in the subsonic range. These include the live measurements of static and total pressures during testing, the static and total pressure calibration processes, and the prediction model error of both the static and total pressure calibration models. In the supersonic range, the prediction model error for the total pressure calibration model is the dominant contributor to  $B_{Q_{ts}}$ .

Scenario 2 (Figure 34) introduces significant contributions to  $B_{Q_{ts}}$  from the static and total pressure measurements and from the static and total pressure calibration processes. Contributions from the static and total pressure prediction model errors are reduced when compared to scenario 3. Live pressure measurements, both static and total, and the static and total pressure calibration processes contribute more significantly as Mach number increases.

In scenario 1 (Figure 35), the contribution from the static pressure prediction model error is reduced significantly. The total pressure prediction model error and measurements of static and total pressures are the primary contributors. There are significant contributions from the static and total pressure calibrations as well.

Table XIV summarizes the results of the Monte Carlo simulation for the calculation of  $q_{ts}$ .

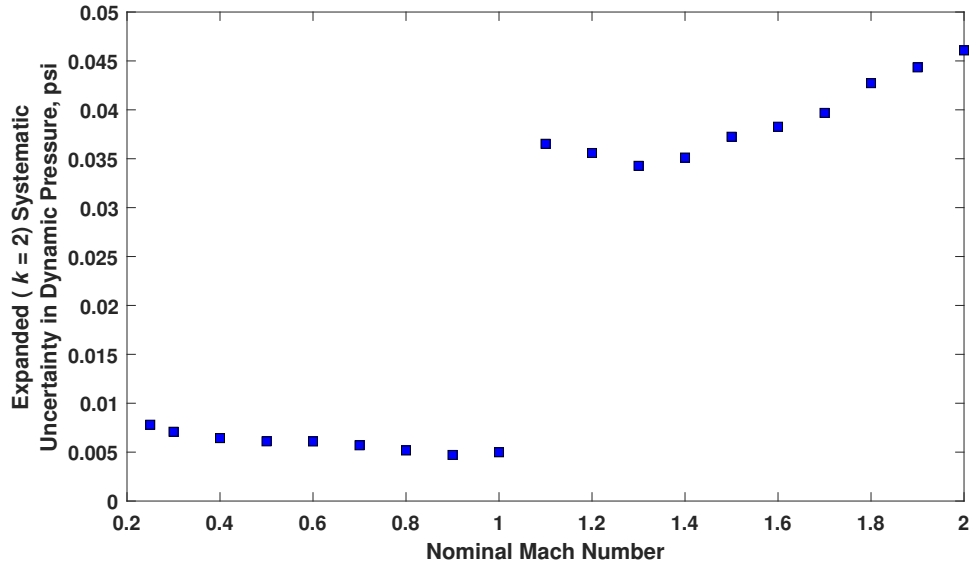


Figure 32. Systematic uncertainty in  $Q_{ts}$  as a function of nominal Mach number for test section porosity configuration 1.

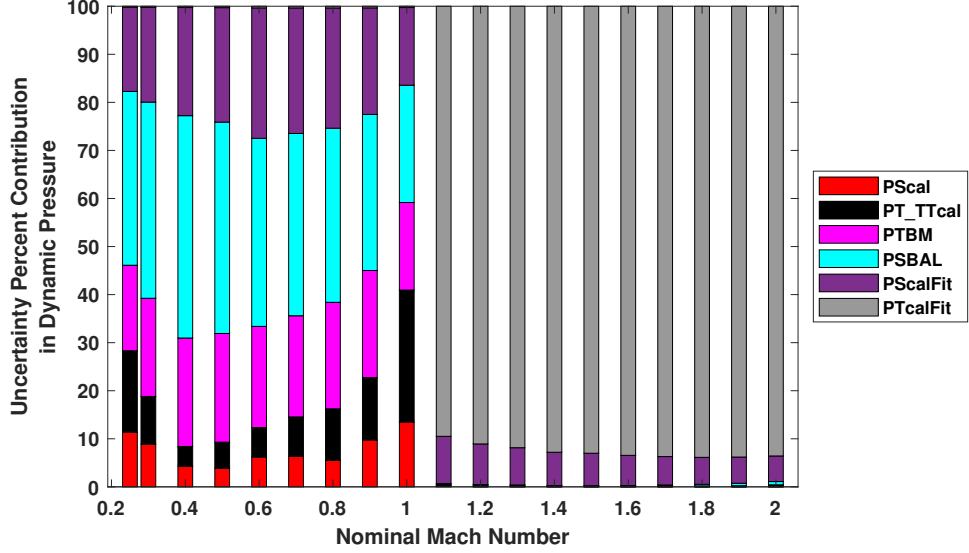


Figure 33. Systematic UPC of  $Q_{ts}$  as a function of nominal Mach number for scenario 3, test section porosity configuration 1.

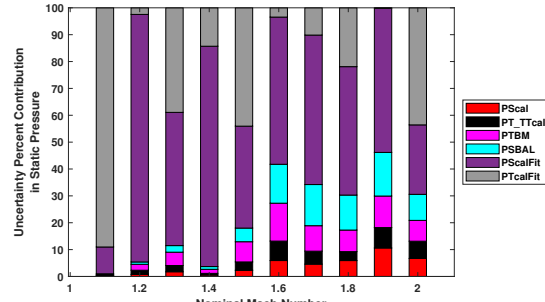


Figure 34. Systematic UPC of  $Q_{ts}$  as a function of nominal Mach number for scenario 2, test section porosity configuration 1.

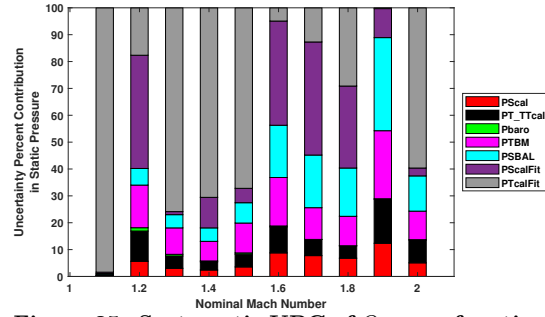


Figure 35. Systematic UPC of  $Q_{ts}$  as a function of nominal Mach number for scenario 1, test section porosity configuration 1.

TABLE XIV. SUMMARY OF SYSTEMATIC UNCERTAINTY RESULTS FOR CALCULATED DYNAMIC PRESSURE, SCENARIO 3, TEST SECTION POROSITY CONFIGURATION 1

Nominal Mach	Typical $Q_{ts}$ psia	$B_{Q_{ts}}$ psia $k=2$	$B_{Q_{ts}}$ UPC due to $b_{P_{S,cal}}$	$B_{Q_{ts}}$ UPC due to $b_{P_T-T_{T,cal}}$	$B_{Q_{ts}}$ UPC due to $b_{P_{T,bm}}$	$B_{Q_{ts}}$ UPC due to $b_{P_{S,bal}}$	$B_{Q_{ts}}$ UPC due to $b_{P_{Scal,fit}}$	$B_{Q_{ts}}$ UPC due to $b_{P_{Tcal,fit}}$
0.25	0.6458	0.0078	11.4	16.9	17.8	36.2	17.5	0.2
0.40	1.5422	0.0064	4.3	4.1	22.6	46.3	22.5	0.3
0.60	3.4662	0.0061	6.2	6.2	21.0	39.1	27.1	0.3
0.80	5.0734	0.0052	5.5	10.7	22.2	36.2	25.0	0.4
1.00	5.9202	0.0050	13.5	27.5	18.2	24.4	16.2	0.3
1.20	7.3253	0.0356	0.0	0.1	0.2	0.1	8.5	91.1
1.40	7.8826	0.0351	0.0	0.1	0.2	0.0	6.9	92.8
1.60	8.6123	0.0383	0.0	0.1	0.1	0.1	6.3	93.4
1.80	9.1381	0.0427	0.0	0.1	0.0	0.3	5.6	93.9
2.00	9.0322	0.0461	0.0	0.4	0.0	0.7	5.3	93.6

#### 7.2.4 Total Temperature Systematic Uncertainty

Figure 36 shows  $B_{T_{T,ts}}$  over the nominal operating range of the facility, using the generalized curve fit prediction models for subsonic and supersonic operations. From M 0.25 to M 0.4,  $B_{T_{T,ts}}$  decreases from 1.17 °R to 1.0 °R.  $B_{T_{T,ts}}$  remains at approximately 1.0 °R from M 0.4 to M 0.8 and then increases to 1.3 °R at M 1.0. In the supersonic range,  $B_{T_{T,ts}}$  decreases from 1.1 °R to approximately 1.0 °R between M 1.1 and M 1.2. Above M 1.2,  $B_{T_{T,ts}}$  is approximately 1.0 °R.

Figure 37 shows a comparison of  $B_{T_{T,ts}}$  over the supersonic operating range, for the prediction model scenarios defined in Table II. The uncertainty in total temperature is not significantly affected by either the flexwall position or the pressure ratio being on- or off-nominal.  $B_{T_{T,ts}}$  is approximately 1.2 °R throughout the supersonic range.

Figures 38, 39 and 40 show the percent contributions of the primary contributors to uncertainty in the calculation of  $Q_{ts}$  for scenarios 3, 2 and 1, respectively.

In scenario 3 (Figure 38) throughout the subsonic and supersonic ranges, the primary contributor to  $B_{T_{T,ts}}$  is the live temperature measurements taken during testing. The next-most dominant contributor is the total temperature calibration process (PT\_TTCal). The total temperature prediction model error and the reference temperature measurement also contribute, but at a much lower percentage.

There is little change in the UPC profile of  $T_{T,ts}$  in scenarios 1 and 2 (Figures 39 and 40, respectively) indicating low impact from using localized curve fit prediction models.

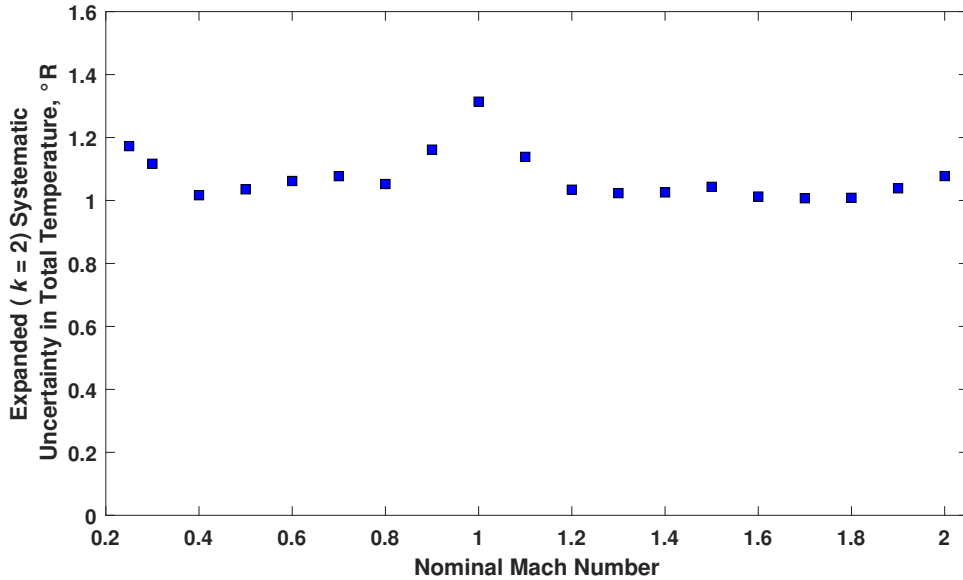


Figure 36. Systematic uncertainty in  $T_{T,ts}$  as a function of nominal Mach number for test section porosity configuration 1.

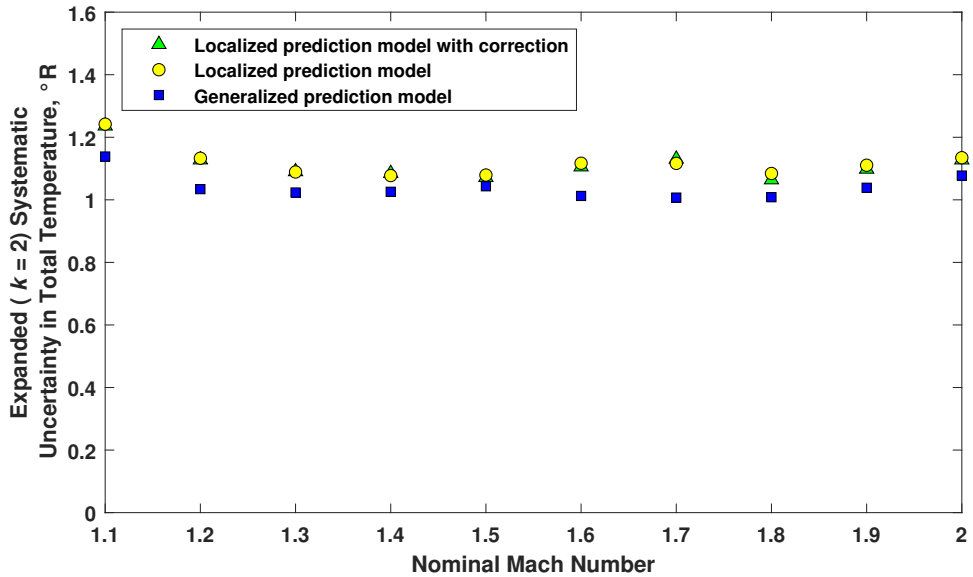


Figure 37. Comparison of systematic uncertainty in  $T_{T,ts}$  for prediction model scenarios 2 and 3 (Table II), as a function of nominal Mach number for test section porosity configuration 1.

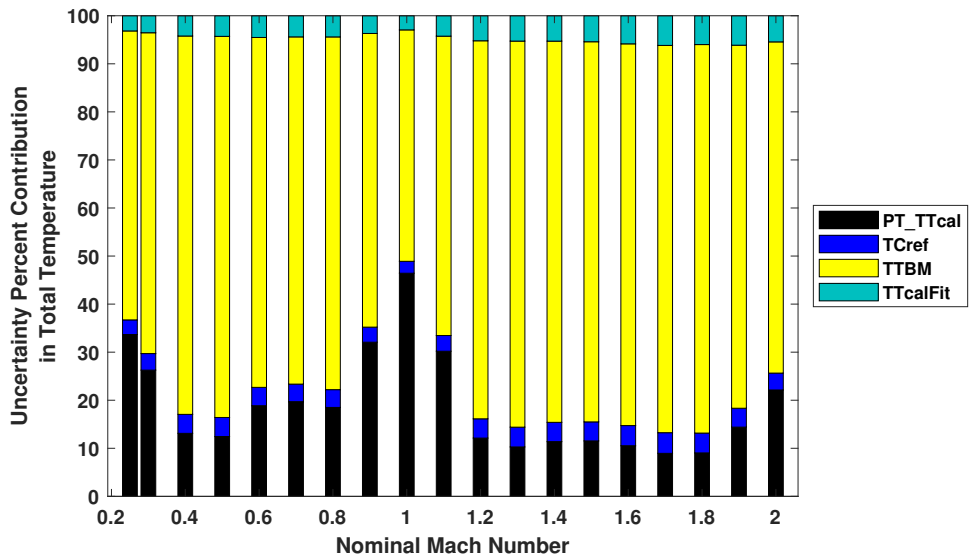


Figure 38. Systematic UPC of  $T_{T,ts}$  as a function of nominal Mach number for scenario 3, test section porosity configuration 1.

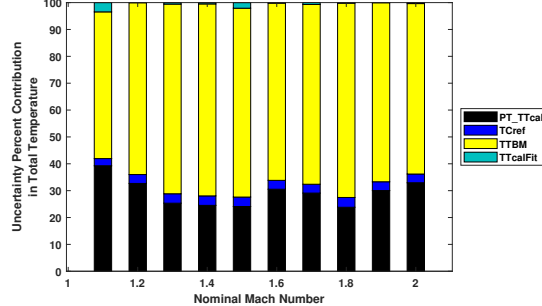


Figure 39. Systematic UPC of  $T_{T,ts}$  as a function of nominal Mach number for scenario 2, test section porosity configuration 1.

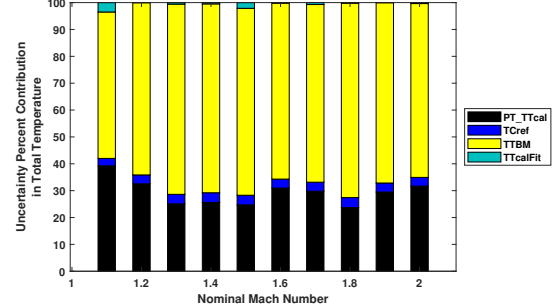


Figure 40. Systematic UPC of  $T_{T,ts}$  as a function of nominal Mach number for scenario 1, test section porosity configuration 1.

Table XV summarizes the results of the Monte Carlo simulation for the calculation of  $T_{T,ts}$ .

TABLE XV. SUMMARY OF SYSTEMATIC UNCERTAINTY RESULTS FOR CALCULATED TEST SECTION TOTAL TEMPERATURE, SCENARIO 3, TEST SECTION POROSITY CONFIGURATION 1

Nominal Mach	Typical $T_{T,ts}$ °R	$B_{T_{T,ts}}$ °R $k=2$	$B_{T_{T,ts}}$ UPC due to $b_{PT-TT,cal}$	$B_{T_{T,ts}}$ UPC due to $b_{TC,ref}$	$B_{T_{T,ts}}$ UPC due to $b_{T_{T,bm}}$	$B_{T_{T,ts}}$ UPC due to $b_{T_{cal,fit}}$
0.25	546	1.17	33.7	3.0	60.1	3.2
0.40	554	1.02	13.1	3.9	78.7	4.2
0.60	589	1.06	18.9	3.8	72.8	4.5
0.80	595	1.05	18.5	3.7	73.4	4.4
1.00	591	1.31	46.4	2.5	48.2	2.9
1.20	600	1.03	12.1	4.0	78.7	5.2
1.40	608	1.03	11.4	4.0	79.3	5.3
1.60	624	1.01	10.5	4.2	79.4	5.8
1.80	626	1.01	9.0	4.1	80.8	6.0
2.00	650	1.08	22.1	3.5	68.9	5.4

### 7.2.5 Static Temperature Systematic Uncertainty

Figure 41 shows  $B_{T_{S,ts}}$  over the nominal operating range of the facility, using the generalized curve fit prediction models for subsonic and supersonic operations. In the subsonic range,  $B_{T_{S,ts}}$  follows a similar profile to  $B_{T_{T,ts}}$  shown in Figure 36.  $B_{T_{S,ts}}$  increases, nonlinearly, from about 1.0 °R to 2.3 °R through the supersonic range.

Figures 42, 43 and 44 show the percent contributions of the primary contributors to uncertainty in the calculation of  $T_{T,ts}$  for scenarios 3, 2 and 1, respectively.

In scenario 3 (Figure 42) in the subsonic range, the primary contributor to  $B_{T_{S,ts}}$  is the live temperature measurements taken during testing. Other contributors include the total temperature calibration process, the total temperature prediction model error and the reference temperature measurement. In the supersonic range, as Mach number increases, the contribution from the live temperature measurements decreases, and the static pressure prediction model error becomes the increasingly dominant contributor to  $B_{T_{S,ts}}$ . The total pressure prediction model error, total temperature prediction model error and the total temperature calibration process also contribute.

In scenario 2 (Figure 43), the contribution to  $B_{T_{S,ts}}$  due to the total temperature measurements is reduced, although it is still the most dominant contributor. Contributions from the static pressure prediction model error and the total temperature calibration process are also significant contributors.

In scenario 1 (Figure 44), the total temperature measures are still the dominant contributor to  $B_{T_{S,ts}}$ , but the contribution from the static pressure prediction model is mostly eliminated. Significant contributions from the total temperature calibration process are also prevalent.

Table XVI summarizes the results of the Monte Carlo simulation for the calculation of  $T_{S,ts}$ .

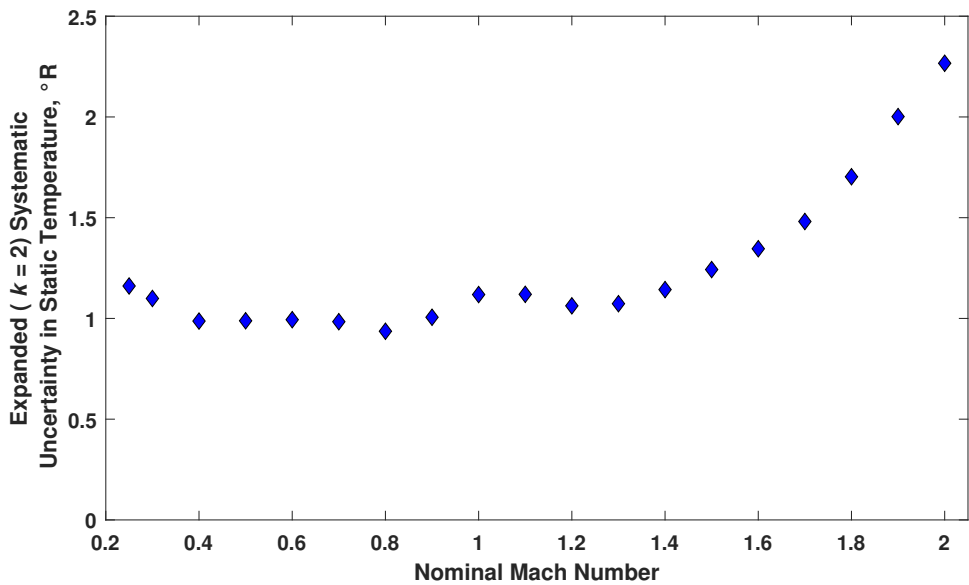


Figure 41. Systematic uncertainty in  $T_{S,ts}$  as a function of nominal Mach number for test section porosity configuration 1.

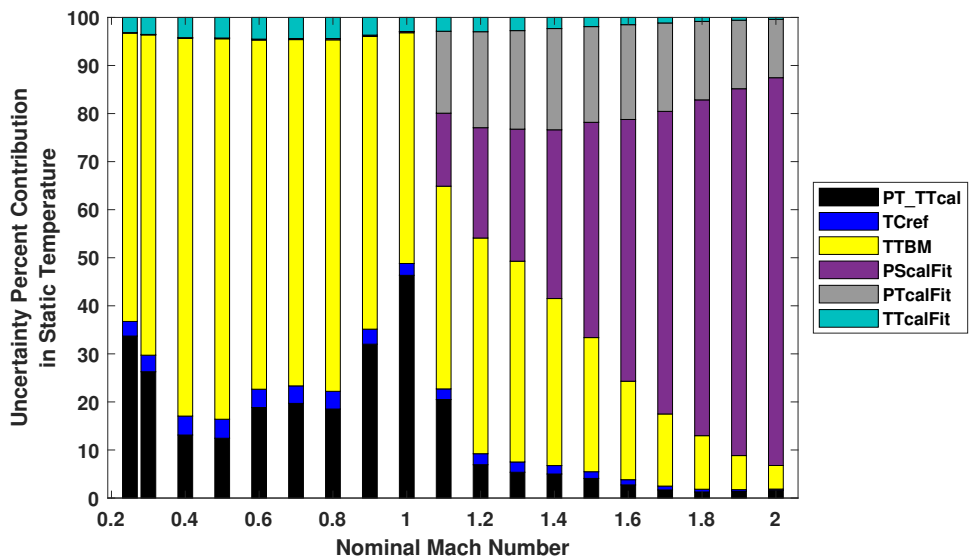


Figure 42. Systematic UPC of  $T_{S,ts}$  as a function of nominal Mach number for scenario 3, test section porosity configuration 1.

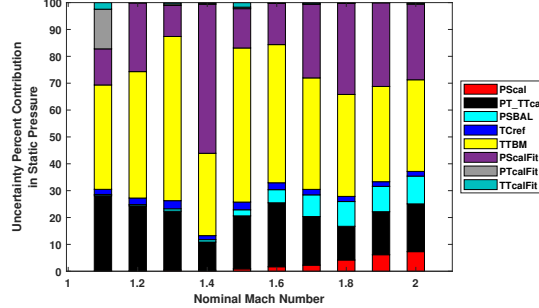


Figure 43. Systematic UPC of  $T_{S,ts}$  as a function of nominal Mach number for scenario 2, test section porosity configuration 1.

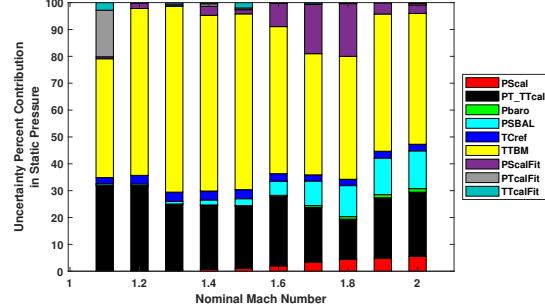


Figure 44. Systematic UPC of  $T_{S,ts}$  as a function of nominal Mach number for scenario 1, test section porosity configuration 1.

TABLE XVI. SUMMARY OF SYSTEMATIC UNCERTAINTY RESULTS FOR CALCULATED STATIC TEMPERATURE, SCENARIO 3, TEST SECTION POROSITY CONFIGURATION 1

Nominal Mach	Typical $T_{S,ts}$ °R	$B_{T_{S,ts}}$ °R $k=2$	$B_{T_{S,ts}}$ UPC	$B_{T_{S,ts}}$ UPC due to $b_{P_T-T_{T,cal}}$	$B_{T_{S,ts}}$ UPC due to $b_{T_{C,ref}}$	$B_{T_{S,ts}}$ UPC due to $b_{T_{T,bm}}$	$B_{T_{S,ts}}$ UPC due to $b_{P_{Scal,fit}}$	$B_{T_{S,ts}}$ UPC due to $b_{P_{Tcal,fit}}$	$B_{T_{S,ts}}$ UPC due to $b_{T_{Tcal,fit}}$
0.25	540	1.16	33.7	3.0	60.0	0.1	0.0	3.2	
0.40	537	0.99	13.1	3.9	78.6	0.1	0.0	4.2	
0.60	549	0.99	18.8	3.8	72.6	0.2	0.0	4.5	
0.80	528	0.94	18.5	3.7	73.1	0.3	0.0	4.4	
1.00	501	1.12	46.3	2.5	48.0	0.3	0.0	2.9	
1.20	469	1.06	6.9	2.3	44.9	23.0	20.0	3.0	
1.40	445	1.14	5.0	1.8	34.8	35.1	21.1	2.3	
1.60	420	1.35	2.7	1.1	20.5	54.5	19.7	1.5	
1.80	383	1.70	1.3	0.6	11.1	69.9	16.3	0.8	
2.00	361	2.27	1.6	0.3	4.9	80.7	12.2	0.4	

### 7.2.6 Test Section Air Speed Systematic Uncertainty

Figure 45 shows  $B_{U_{ts}}$  over the nominal operating range of the facility, using the generalized curve fit prediction models (scenario 3) for subsonic and supersonic operations. In the subsonic range,  $B_{U_{ts}}$  decreases from 1.8 ft/s to 0.9 ft/s from M 0.25 to M 0.6. It then increases to 1.3 ft/s at M 1.0. In the supersonic range,  $B_{U_{ts}}$  increases nonlinearly from 3.5 ft/s to 7.2 ft/s as Mach number increases from M 1.1 to M 2.0.

Figures 46 47 and 48 show the percent contributions of the primary contributors to uncertainty in the calculation of  $U_{ts}$  for scenarios 3, 2 and 1, respectively.

Scenario 3 (Figure 46) shows the percent contributions of the primary contributors to uncertainty in the calculation of  $U_{ts}$ . In the subsonic range, below M 0.6, the live static and total pressure measurements have a larger contribution than the total temperature measurements. Above M 0.6 and up to M 1.0, total temperature measurement becomes the more significant contributor. Other contributors include both static and total pressure calibration processes, measurement of the reference temperature, and the error contributed by the prediction models for static pressure, total pressure, and total temperature. In the supersonic range, the prediction model error from the static and total pressure curve fits are the dominant contributors to  $B_{U_{ts}}$ .

In scenario 2 (Figure 47), the contributions to  $B_{U_{ts}}$  from the static pressure and total temperature measurements are reduced. The dominant contributor becomes the static pressure prediction model error.

In scenario 1 (Figure 48), the contribution from the static pressure prediction model error is reduced significantly. The temperature measurements become the dominant contributor, with significant contributions from the static pressure measurements, total pressure/temperature calibration process and the static pressure calibration process.

Table XVII summarizes the results of the Monte Carlo simulation for the calculation of  $U_{ts}$ .

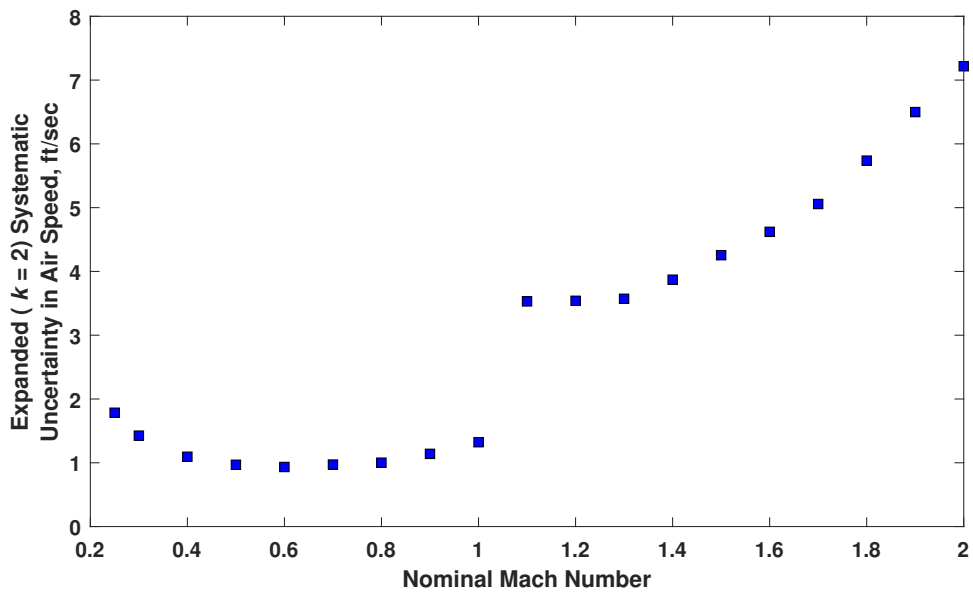


Figure 45. Systematic uncertainty in  $U_{ts}$  as a function of nominal Mach number for test section porosity configuration 1.

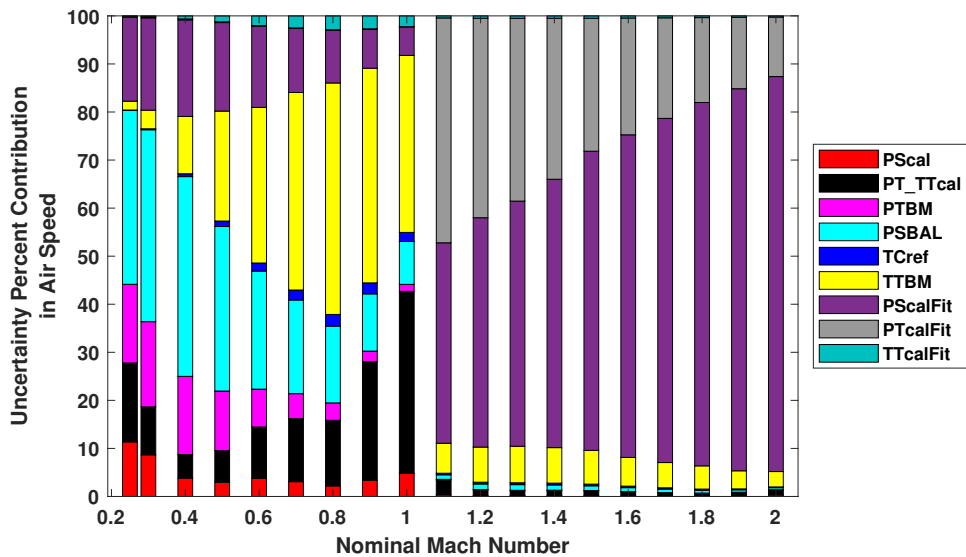


Figure 46. Systematic UPC of  $U_{ts}$  as a function of nominal Mach number for scenario 3, test section porosity configuration 1.

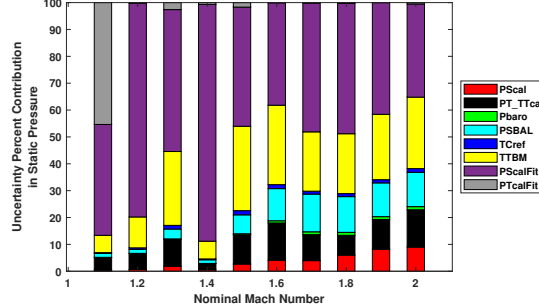


Figure 47. Systematic UPC of  $U_{ts}$  as a function of nominal Mach number for scenario 2, test section porosity configuration 1.

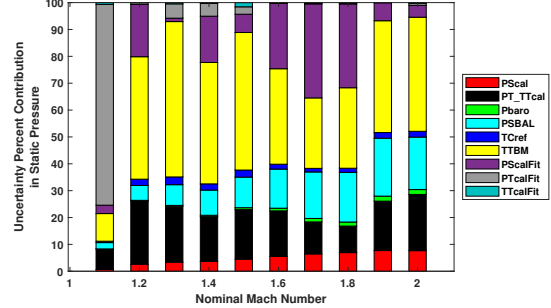


Figure 48. Systematic UPC of  $U_{ts}$  as a function of nominal Mach number for scenario 1, test section porosity configuration 1.

TABLE XVII. SUMMARY OF SYSTEMATIC UNCERTAINTY RESULTS FOR CALCULATED AIR SPEED, SCENARIO 3, TEST SECTION POROSITY CONFIGURATION 1

Nominal Mach	Typical $U_{ts}$ ft/s	$B_{U_{ts}}$ ft/s	$B_{U_{ts}}$ UPC due to $b_{P_{T-T_{cal}}}$	$B_{U_{ts}}$ UPC due to $b_{P_{T-T_{bm}}}$	$B_{U_{ts}}$ UPC due to $b_{P_{S,bm}}$	$B_{U_{ts}}$ UPC due to $b_{P_{C,ref}}$	$B_{U_{ts}}$ UPC due to $b_{T_{T,bm}}$	$B_{U_{ts}}$ UPC due to $b_{P_{Scal,fit}}$	$B_{U_{ts}}$ UPC due to $b_{P_{Tcal,fit}}$	$B_{U_{ts}}$ UPC due to $b_{T_{cal,fit}}$
0.25	286	1.7846	11.4	16.4	36.2	0.1	1.8	17.5	0.2	0.1
0.40	455	1.0947	3.8	4.9	41.6	0.6	11.9	20.1	0.2	0.6
0.60	689	0.9338	3.8	10.7	24.5	1.7	32.4	16.9	0.1	2.0
0.80	901	1.0017	2.2	13.7	16.0	2.4	48.2	11.0	0.1	2.9
1.00	1043	1.3224	4.8	37.9	1.5	8.9	36.8	5.9	0.0	2.3
1.20	1256	3.5398	0.2	1.2	0.1	1.2	0.4	7.3	47.7	41.5
1.40	1398	3.8704	0.2	1.1	0.1	1.1	0.4	7.4	55.8	33.5
1.60	1566	4.6209	0.2	0.8	0.0	0.8	0.3	6.0	67.1	24.3
1.80	1707	5.7374	0.1	0.6	0.0	0.6	0.2	4.8	75.6	17.7
2.00	1862	7.2168	0.3	1.1	0.0	0.4	0.2	3.2	82.2	12.4

### 7.2.7 Reynolds Number Systematic Uncertainty

Figure 49 shows  $B_{RE_{ft}}$  over the nominal operating range of the facility, using the generalized curve fit prediction models for subsonic and supersonic operations. In the subsonic range,  $B_{RE_{ft}}$  decreases from  $0.01 \cdot 10^6 \text{ ft}^{-1}$  to  $0.008 \cdot 10^6 \text{ ft}^{-1}$  from M 0.25 to M 0.4 and then increases to  $0.013 \cdot 10^6 \text{ ft}^{-1}$  at M 1.0. In the supersonic range,  $B_{RE_{ft}}$  ranges from  $0.02 \cdot 10^6 \text{ ft}^{-1}$  to  $0.1 \cdot 10^6 \text{ ft}^{-1}$  as Mach number increases from M 1.1 to M 2.0.

Figures 50, 51 and 52 show the percent contributions of the primary contributors to uncertainty in the calculation of  $RE_{ft}$  for scenarios 3, 2 and 1, respectively.

In scenario 3 (Figure 50), in the subsonic range, below M 0.4, the live measurements of static and total pressure and total temperature all contribute strongly to  $B_{RE_{ft}}$ . Both the static and total calibration processes contribute below M 0.4. Above M 0.4 and up to M 1.0, the total temperature measurement becomes the most significant contributor and the total pressure calibration process contribution increases as Mach number increases. In the supersonic range, the prediction model error from the total pressure curve fit is the dominant contributor to  $B_{RE_{ft}}$ . The total temperature measurements also have a significant contribution in this range.

In both scenarios 1 and 2 (Figures 52 and 51, respectively), the contributions from both static and total pressure prediction model errors are significantly reduced. The total temperature measurements are the dominant contributors to  $B_{RE_{ft}}$  in both cases. The total pressure/temperature calibration process is the next most dominant contributor to  $B_{RE_{ft}}$ .

Table XVIII summarizes the results of the Monte Carlo simulation for the calculation of  $RE_{ft}$ .

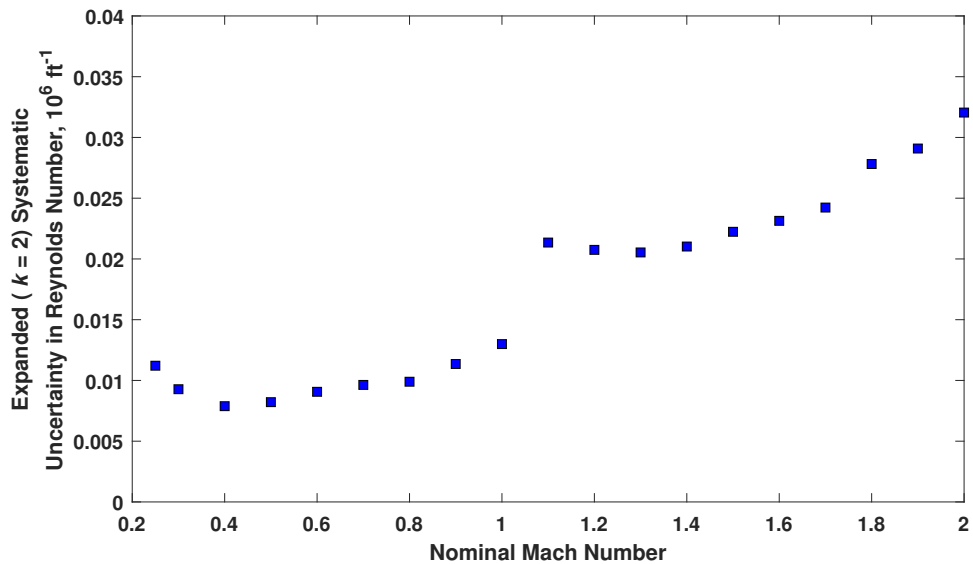


Figure 49. Systematic uncertainty in  $RE_{ft}$  as a function of nominal Mach number for test section porosity configuration 1.

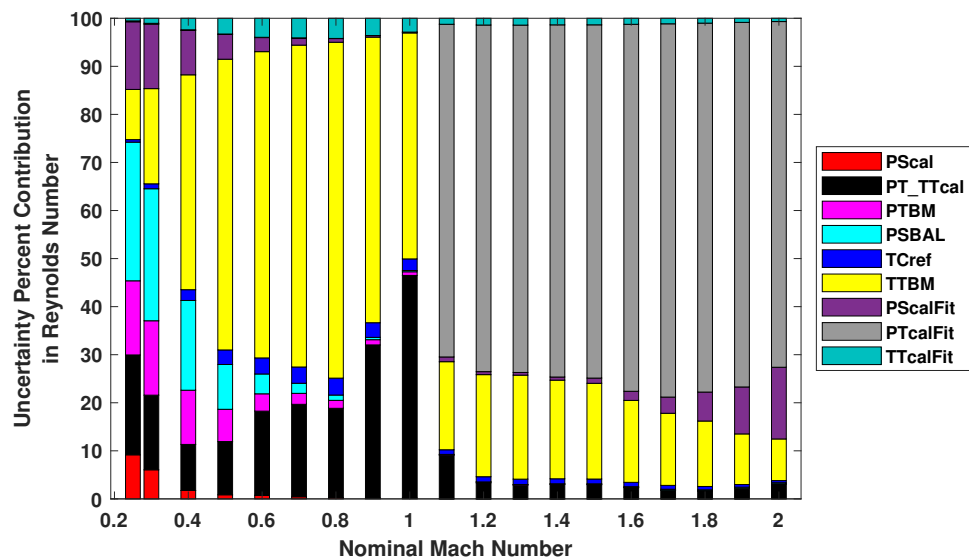


Figure 50. Systematic UPC of  $RE_{ft}$  as a function of nominal Mach number for scenario 3, test section porosity configuration 1.

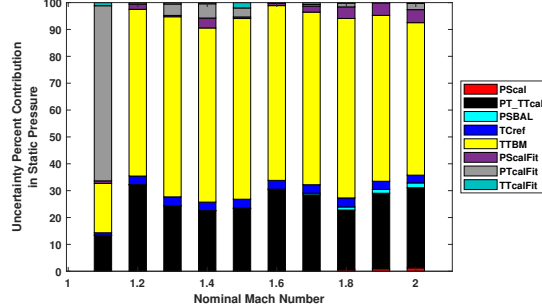


Figure 51. Systematic UPC of  $RE_{ft}$  as a function of nominal Mach number for scenario 2, test section porosity configuration 1.

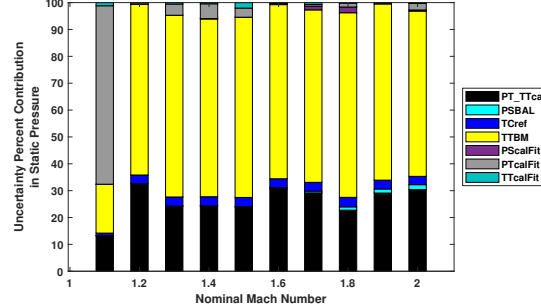


Figure 52. Systematic UPC of  $RE_{ft}$  as a function of nominal Mach number for scenario 1, test section porosity configuration 1.

TABLE XVIII. SUMMARY OF SYSTEMATIC UNCERTAINTY RESULTS FOR CALCULATED REYNOLDS NUMBER, SCENARIO 3, TEST SECTION POROSITY CONFIGURATION 1

Nominal Mach	Typical $RE_{ft}$ $10^6 ft^{-1}$	$BRE_{ft}$ $10^6 ft^{-1}$ $k=2$	$BRE_{ft}$ UPC due to $b_{PS,cal}$	$BRE_{ft}$ UPC due to $b_{PT-T_{T,cal}}$	$BRE_{ft}$ UPC due to $b_{PT,bm}$	$BRE_{ft}$ UPC due to $b_{PS,bal}$	$BRE_{ft}$ UPC due to $b_{TC,ref}$	$BRE_{ft}$ UPC due to $b_{T_{T,bm}}$	$BRE_{ft}$ UPC due to $b_{PScal,fit}$	$BRE_{ft}$ UPC due to $b_{PTcal,fit}$	$BRE_{ft}$ UPC due to $b_{TTcal,fit}$
0.25	1.69	0.011	9.2	20.8	15.4	28.8	0.5	10.4	14.1	0.2	0.5
0.40	2.54	0.008	1.7	9.6	11.3	18.7	2.2	44.7	9.2	0.1	2.4
0.60	3.71	0.009	0.7	17.5	3.6	4.1	3.3	63.7	2.9	0.1	4.0
0.80	4.28	0.010	0.3	18.6	1.7	1.1	3.5	69.9	0.8	0.0	4.2
1.00	4.49	0.013	0.2	46.3	0.8	0.3	2.4	47.0	0.2	0.0	2.9
1.20	4.86	0.021	0.0	3.3	0.2	0.0	1.1	21.2	0.6	72.1	1.4
1.40	4.90	0.021	0.0	3.0	0.1	0.0	1.0	20.5	0.7	73.3	1.4
1.60	5.02	0.023	0.0	2.3	0.1	0.1	0.9	17.1	1.9	76.4	1.3
1.80	5.27	0.028	0.0	1.6	0.0	0.2	0.7	13.6	6.0	76.8	1.0
2.00	5.02	0.032	0.1	3.0	0.0	0.2	0.4	8.7	14.9	71.9	0.7

## 8 Conclusions

Uncertainty in the  $8 \times 6$  SWT is best characterized by modeling the expanded systematic uncertainty in VOIs using the Monte Carlo method of uncertainty propagation. Prediction models were developed separately for subsonic and supersonic operations due to the differing nature of the response between the two modes of operation. The results are summarized in Table XIX.

**TABLE XIX. SUMMARY OF SYSTEMATIC UNCERTAINTY RESULTS FOR  $8 \times 6$  SWT VOIs (Coverage Factor ( $k = 2$ ), Level of Confidence: 95 percent)**

Variable of Interest	Subsonic Uncertainty	Supersonic Uncertainty		
		Generalized	Localized	On-nominal
Mach Number	0.002	0.004-0.01	0.002-0.005	0.001-0.003
Static Pressure, psi	0.007	0.03-0.04	0.01-0.04	0.005-0.01
Total Pressure, psi	0.005	0.06-0.3	0.007-0.06	0.006-0.06
Total Temperature, $^{\circ}$ R	1.0-1.3	1.0-1.1	1.1-1.2	1.1-1.2
Dynamic Pressure, psi	0.005-0.008	0.03-0.05		
Static Temperature, $^{\circ}$ R	0.9-1.2	1.1-2.3		
Reynolds Number $10^6 \text{ ft}^{-1}$	0.008-0.01	0.02-0.03		
Free Stream Air Speed, ft/s	0.9-1.8	3.5-7.2		

In the subsonic range uncertainty is relatively linear for VOIs that are functions of pressure only, such as static pressure, total pressure, Mach number and dynamic pressure. VOIs that are functions of both pressure and temperature, such as static temperature, air speed and Reynolds number, show some nonlinearity in subsonic uncertainty. Uncertainty in the subsonic range is typically lower than in the supersonic range and generalized prediction models covering the entire subsonic range are applicable.

In the supersonic range, uncertainty prediction models were developed for local, on-nominal and general scenarios (Table II) for the primary VOI,  $M_{ts}$ , and for  $P_{S,ts}$ ,  $P_{T,ts}$ ,  $T_{T,ts}$ . For  $P_{S,ts}$ ,  $P_{T,ts}$ , and  $M_{ts}$ , uncertainty is significantly reduced when both the flexwall position and  $R_{S,bal,bm}$  are within defined localized boundaries, and prediction models localized to each specific Mach number target are used to calculate VOIs. Uncertainty in  $M_{ts}$  is lowest when  $R_{S,bal,bm}$  is held to within  $\pm 0.0005$  of the nominal target condition and an additional correction factor is added to the static pressure prediction (Figures 17, 23, 28). The uncertainty in  $T_{T,ts}$  is essentially the same whether using the generalized prediction model covering the entire supersonic range, or using localized prediction models (Figure 37).

The benefit of applying localized curve fit prediction models is highlighted in the UPC charts for each VOI. The contributions from errors in the prediction models are reduced by using more accurate localized models, revealing other significant contributors.

If an improved understanding of random uncertainty is of interest, it is recommended that a larger repeat data set be collected during the next characterization test. A minimum of six repeat data sets is recommended. In addition, when running the repeat data sets, it is suggested that detailed records of all settings not normally collected in the data set be recorded in some fashion. This will aid in troubleshooting unusual results as seen in  $B_{P_{S,ts}}$ , at 1.4M, during the 2019 Characterization Test (Ref. [1]).

Look-up tables of the uncertainty analysis results for the  $8 \times 6$  SWT are presented in Tables XX, XXI and XXII.

TABLE XX. UNCERTAINTY ( $k=2$ ) LOOK-UP TABLE FOR THE  $8 \times 6$  SUPERSONIC WIND TUNNEL SUPERSONIC LOCALIZED PREDICTION MODEL, WITH STATIC PRESSURE CORRECTION<sup>1</sup>

$M_{ts}$ unitless	$B_{M_{ts}}$ unitless	$P_{S,ts}$ psia	$B_{P_{S,ts}}$ psia	$P_{T,ts}$ psia	$B_{P_{T,ts}}$ psia	$Q_{ts}$ psia	$B_{Q_{ts}}$ psia	$T_{T,ts}$ $^{\circ}R$	$B_{T_{T,ts}}$ $^{\circ}R$	$T_{S,ts}$ $^{\circ}R$	$B_{T_{S,ts}}$ $^{\circ}R$	$RE_{ft}$ $10^6 ft^{-1}$	$B_{RE_{ft}}$ $10^6 ft^{-1}$	$U_{ts}$ ft/s	$B_{U_{ts}}$ ft/s
1.08	0.0028	8.39	0.0081	17.42	0.0573	6.82	0.0342	599	1.24	486	1.11	4.75	0.022	1164	2.74
1.18	0.0009	7.48	0.0084	17.75	0.0055	7.33	0.0041	600	1.13	469	0.90	4.87	0.012	1257	1.41
1.25	0.0007	6.89	0.0052	17.89	0.0103	7.56	0.0054	600	1.09	457	0.84	4.91	0.012	1311	1.32
1.36	0.0013	6.14	0.0084	18.36	0.0133	7.90	0.0064	608	1.08	445	0.83	4.91	0.012	1401	1.55
1.46	0.0011	5.59	0.0066	19.29	0.0125	8.31	0.0050	616	1.07	433	0.78	4.97	0.012	1486	1.51
1.55	0.0019	5.08	0.0105	20.15	0.0155	8.58	0.0039	624	1.11	421	0.82	5.00	0.012	1562	1.89
1.66	0.0028	4.57	0.0133	21.35	0.0283	8.85	0.0048	632	1.13	407	0.88	5.04	0.012	1645	2.30
1.79	0.0030	4.09	0.0121	23.18	0.0388	9.18	0.0047	626	1.06	381	0.83	5.29	0.012	1714	2.25
1.89	0.0022	3.63	0.0076	24.06	0.0320	9.11	0.0028	647	1.10	377	0.74	5.05	0.012	1801	1.95
1.99	0.0023	3.24	0.0066	25.06	0.0388	9.01	0.0040	650	1.13	362	0.73	5.00	0.012	1859	1.99

---

<sup>1</sup>Flexwall position within  $\pm 2$  degrees of nominal position and  $R_{S,bal,bm}$  within  $\pm 0.0005$  of nominal pressure ratio.

**TABLE XXI. UNCERTAINTY ( $k=2$ ) LOOK-UP TABLE FOR THE  $8 \times 6$  SUPERSONIC WIND TUNNEL SUPERSONIC LOCALIZED PREDICTION MODEL<sup>1</sup>**

$M_{ts}$ unitless	$B_{M_{ts}}$ unitless	$P_{S,ts}$ psia	$B_{P_{S,ts}}$ psia	$P_{T,ts}$ psia	$B_{P_{T,ts}}$ psia	$Q_{ts}$ psia	$B_{Q_{ts}}$ psia	$T_{T,ts}$ $^{\circ}R$	$B_{T_{T,ts}}$ $^{\circ}R$	$T_{S,ts}$ $^{\circ}R$	$B_{T_{S,ts}}$ $^{\circ}R$	$RE_{ft}$ $10^6 ft^{-1}$	$B_{RE_{ft}}$ $10^6 ft^{-1}$	$U_{ts}$ ft/s	$B_{U_{ts}}$ ft/s
1.08	0.0038	8.39	0.0266	17.42	0.0580	6.82	0.0363	599	1.24	486	1.19	4.75	0.022	1164	3.54
1.18	0.0030	7.48	0.0268	17.75	0.0069	7.33	0.0107	600	1.13	469	1.02	4.87	0.012	1257	2.73
1.25	0.0019	6.88	0.0150	17.89	0.0112	7.56	0.0075	600	1.09	457	0.89	4.91	0.012	1312	1.91
1.36	0.0053	6.13	0.0376	18.36	0.0248	7.90	0.0140	608	1.08	444	1.22	4.91	0.012	1402	4.18
1.46	0.0021	5.58	0.0129	19.29	0.0162	8.31	0.0061	616	1.08	433	0.85	4.97	0.012	1486	1.97
1.55	0.0023	5.07	0.0126	20.15	0.0182	8.58	0.0044	624	1.12	421	0.85	5.00	0.012	1562	2.09
1.66	0.0033	4.58	0.0155	21.34	0.0327	8.85	0.0054	632	1.12	407	0.92	5.04	0.012	1644	2.53
1.79	0.0037	4.10	0.0151	23.16	0.0479	9.18	0.0054	626	1.08	382	0.92	5.29	0.013	1713	2.62
1.89	0.0037	3.63	0.0128	24.08	0.0541	9.11	0.0041	647	1.11	377	0.91	5.05	0.012	1802	2.56
1.99	0.0037	3.24	0.0108	25.08	0.0610	9.01	0.0047	650	1.13	362	0.87	5.00	0.013	1859	2.50

---

<sup>1</sup>Flexwall position within  $\pm 2$  degrees of nominal position and  $R_{S,bal,bm}$  within upper and lower limits of nominal pressure ratio range for the target Mach number.

**TABLE XXII. UNCERTAINTY ( $k=2$ ) LOOK-UP TABLE FOR THE  $8 \times 6$  SUPERSONIC WIND TUNNEL GENERALIZED PREDICTION MODEL<sup>1</sup>**

$M_{ts}$ unitless	$B_{M_{ts}}$ unitless	$P_{S,ts}$ psia	$B_{P_{S,ts}}$ psia	$P_{T,ts}$ psia	$B_{P_{T,ts}}$ psia	$Q_{ts}$ psia	$B_{Q_{ts}}$ psia	$T_{T,ts}$ $^{\circ}R$	$B_{T_{T,ts}}$ $^{\circ}R$	$T_{S,ts}$ $^{\circ}R$	$B_{T_{S,ts}}$ $^{\circ}R$	$RE_{ft}$ $10^6 ft^{-1}$	$B_{RE_{ft}}$ $10^6 ft^{-1}$	$U_{ts}$ ft/s	$B_{U_{ts}}$ ft/s
0.25	0.0016	14.64	0.0066	15.30	0.0048	0.65	0.0078	546	1.17	540	1.16	1.69	0.011	286	1.78
0.30	0.0012	14.35	0.0064	15.27	0.0042	0.90	0.0071	548	1.12	538	1.10	1.98	0.009	340	1.43
0.40	0.0009	13.71	0.0062	15.32	0.0038	1.54	0.0064	554	1.02	537	0.99	2.54	0.008	455	1.09
0.50	0.0007	13.38	0.0062	15.87	0.0039	2.35	0.0061	564	1.04	537	0.99	3.09	0.008	568	0.97
0.60	0.0006	13.78	0.0065	17.57	0.0040	3.47	0.0061	589	1.06	549	0.99	3.71	0.009	689	0.93
0.70	0.0006	12.65	0.0065	17.55	0.0041	4.35	0.0057	595	1.08	542	0.98	4.05	0.010	800	0.97
0.80	0.0006	11.32	0.0064	17.26	0.0043	5.07	0.0052	595	1.05	528	0.94	4.28	0.010	901	1.00
0.90	0.0006	9.98	0.0065	16.87	0.0044	5.66	0.0047	592	1.16	509	1.01	4.44	0.011	995	1.14
0.95	0.0007	9.36	0.0068	16.74	0.0054	5.92	0.0050	591	1.31	501	1.12	4.49	0.013	1043	1.32
1.08	0.0038	8.40	0.0267	17.43	0.0583	6.82	0.0365	599	1.14	486	1.12	4.75	0.021	1164	3.53
1.18	0.0040	7.48	0.0269	17.74	0.0633	7.33	0.0356	600	1.03	469	1.06	4.86	0.021	1256	3.54
1.25	0.0042	6.89	0.0273	17.88	0.0655	7.55	0.0343	600	1.02	457	1.07	4.91	0.021	1311	3.57
1.35	0.0049	6.16	0.0281	18.33	0.0753	7.88	0.0351	608	1.03	445	1.14	4.90	0.021	1398	3.87
1.46	0.0057	5.58	0.0296	19.32	0.0917	8.32	0.0373	617	1.04	432	1.24	4.98	0.022	1487	4.25
1.56	0.0066	5.06	0.0313	20.26	0.1089	8.61	0.0383	624	1.01	420	1.35	5.02	0.023	1566	4.62
1.67	0.0077	4.56	0.0320	21.36	0.1337	8.85	0.0397	632	1.01	407	1.48	5.03	0.024	1646	5.06
1.78	0.0095	4.12	0.0350	22.95	0.1764	9.14	0.0427	626	1.01	383	1.70	5.27	0.028	1707	5.74
1.89	0.0114	3.64	0.0367	23.98	0.2222	9.09	0.0443	647	1.04	378	2.00	5.03	0.029	1799	6.50
2.00	0.0136	3.23	0.0373	25.24	0.2842	9.03	0.0461	650	1.08	361	2.27	5.02	0.032	1862	7.22

<sup>1</sup>Flexwall position and  $R_{S,bal,bm}$  outside of localized boundary setpoints.

## References

1. Johnson, A. M. & Rinehart, D. A.: Characterization of the NASA Glenn Research Center 8- by 6-Foot Supersonic Wind Tunnel (2019 Test). Calibration Report NASA/CR-20205006102 (National Aeronautics and Space Administration, Apr. 2021).
2. Soeder, R. H.: NASA Glenn 8-by 6-foot Supersonic Wind Tunnel User Manual. Technical Memorandum NASA TM 105771 (National Aeronautics and Space Administration, 1993).
3. American Society of Mechanical Engineers: Test Uncertainty. Standard ASME PTC 19.1-2013 (2014).
4. American Institute of Aeronautics and Astronautics: Assessment of Experimental Uncertainty with Application to Wind Tunnel Testing. Standard AIAA S-071A-1999 (1999).
5. Coleman, H. W. & Steele, W. G.: Experimentation, Validation and Uncertainty Analysis for Engineers Third (John Wiley and Sons, Inc., 2009).
6. Stephens, J., Hubbard, E., Walter, J., *et al.*: Uncertainty Analysis of the NASA Glenn 8×6 Supersonic Wind Tunnel. Contractor Report NASA/CR-2016-219411 (National Aeronautics and Space Administration, 2016).
7. Joint Committee for Guides in Metrology: Evaluation of Measurement Data - Guide to the Expression of Uncertainty in Measurement. Guide JCGM 100:2008 (International Organization for Standardization, 2008).
8. Rouse, B., Morales, J. & McElroy, J.: Measurement Analysis Tool for Uncertainty in Systems Overview. Contractor Report (National Aeronautics and Space Administration, In Progress).
9. Ames Research Staff: Equations, Tables, and Charts for Compressible Flow. Tech. rep. NACA TR-1135 (National Aeronautics and Space Administration, 1953).





